THE Journal OF THE AMERICAN LEATHER CHEMISTS ASSOCIATION

August 2021 Vol. CXVI, No.8 *JALCA* 116(8), 265–300, 2021

Contents

Distributed by
University of CINCINNATI
LIBRARY PUBLISHING SERVICES

An imprint of the University of Cincinnati Press

ISSN: 0002-9726

Communications for Journal Publication

Manuscripts, Technical Notes and Trade News Releases should contact:
Mr. Steven D. Lange, Journal Editor, 1314 50th Street, Suite 103, Lubbock, TX 79412, USA
E-mail: jalcaeditor@gmail.com Mobile phone: (814) 414-5689

Contributors should consult the Journal Publication Policy at:
http://www.leatherchemists.org/journal_publication_policy.asp

Beamhouse efficiency takes perfect balance.

Making leather on time, on spec and within budget requires a careful balance of chemistry and process. Buckman enables tanneries to master that balance with our comprehensive Beamhouse & Tanyard Systems. They include advanced chemistries that not only protect the hide but also maximize the effectiveness of each process, level out the differences in raw materials and reduce variations in batch processing. The result is cleaner, flatter pelts. More uniform characteristics. And improved area yield.

In addition, we offer unsurpassed expertise and technical support to help solve processing problems and reduce environmental impact with chemistries that penetrate faster, save processing time, improve effluent and enhance safety.

With Buckman Beamhouse & Tanyard Systems, tanneries can get more consistent quality and more consistent savings. Maintain the perfect balance. Connect with a Buckman representative or visit us at **Buckman.com**.

1945 2020 Buckman75

JOURNAL OF THE
AMERICAN LEATHER CHEMISTS ASSOCIATION

Proceedings, Reports, Notices, and News
of the
AMERICAN LEATHER CHEMISTS ASSOCIATION

THE JOURNAL OF THE AMERICAN LEATHER CHEMISTS ASSOCIATION (USPS #019-334) is published monthly by The American Leather Chemists Association, 1314 50th Street, Suite 103, Lubbock, Texas 79412. Telephone (806)744-1798 Fax (806)744-1785. Single copy price: $8.50 members, $17.00 non-member. Subscriptions: $185 for hard copy plus postage and handling of $60 for domestic subscribers and $70 for foreign subscribers; $185 for ezine only; and $205 for hard copy and ezine plus postage and handling of $60 for domestic subscribers and $70 for foreign subscribers.

Periodical Postage paid at Lubbock, Texas and additional mailing offices. Postmaster send change of addresses to The American Leather Chemists Association, 1314 50th Street, Suite 103, Lubbock, Texas 79412.

Website: www.leatherchemists.org E-mail: carol.adcock@ttu.edu

LEATHER

AVELLISYNCO

Selected Dyestuffs

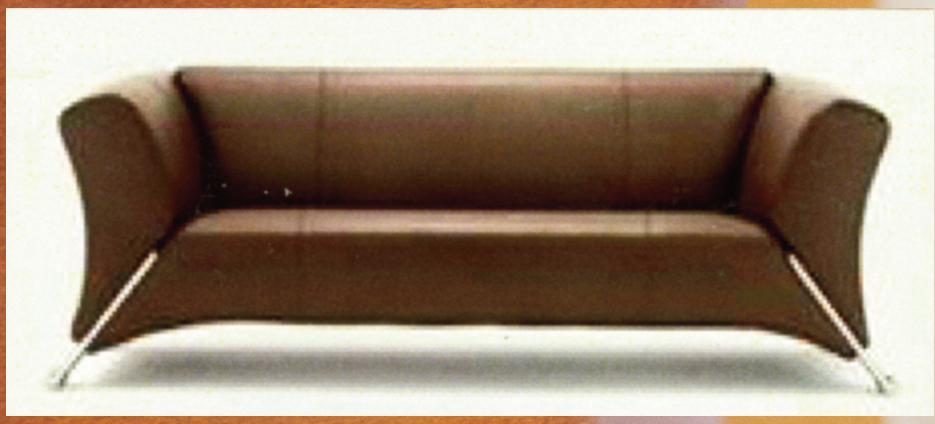

CHEMTAN

17 Noble Farm Drive • Lee, NH 03861 (Office)
57 Hampton Road • Exeter, NH 03833 (Manufacturing)
Tel: (603) 772-3741 • Fax: (603) 772-0796
www.CHEMTAN.com

Research on Sheepskin Contour Extraction Method Based on Computer Vision Measurement Technology

by
Hu Lianhua, Xıang Chengyi* and Zhang Feng
School of Mechanical and Electrical Engineering, Shaanxi University of Science and Technology,
Xi'an, Shaanxi Province, 710021, China

Abstract

Manual trimming of sheepskin is intensive labor, and the working environment is full of rotten smells. The tannery is facing increasingly severe recruitment difficulties. This paper uses computer vision technology to study automatic recognition of sheepskin contours, which is the basis for the subsequent automatic trimming of sheepskin. After observing and analyzing the raw sheepskin images collected by an industrial array camera, a method of sheepskin contour extraction based on computer vision measurement technology is proposed in this paper. This method uses the fast Otsu threshold algorithm based on the pixel set to perform binary image segmentation. Combined with morphological processing for edge defect filling and topology analysis of boundary contour tracking algorithm to extract maximum contour information, it has a pixel-level three-dimensional de-noising preprocessing function and can accurately extract the sheepskin contour in the raw sheepskin image. The experimental results show that using the fast Otsu threshold algorithm proposed in this paper for binary segmentation to extract sheepskin contours, the detection rate is nearly 160% faster than the traditional Otsu algorithm, the edge protection is better, the error segmentation is reduced by nearly 3% and it has good anti-noise performance. It can meet the industrial production requirements of subsequent automatic cutting of sheepskin.

Introduction

China is recognized as a big country in sheepskin production and processing in the world, but it is not a powerful country in production and processing. Compared with developed countries, sheepskin production and processing automation level is relatively low. The tannery in China is still a typical labor-intensive industry. At present, most sheepskin production and processing enterprises mainly use manual cutting for the cleaning of sheep fillet skin. There are problems such as high labor intensity and poor working environment. Companies are facing increasing employment difficulties. In recent years, with the rapid development of computer vision processing technology,[1,2] the use of computer vision processing technology to achieve automatic edge trimming of sheepskin can liberate the production labor force and greatly improve the production and processing efficiency and optimization cost of sheepskin production enterprises. When computer vision processing technology is applied to automatic cutting of sheepskin, the main steps are image acquisition, image segmentation, coordinate extraction and automatic cutting. Image segmentation is an extremely critical step to realize automatic cutting. Therefore, it is the first task to propose an image segmentation algorithm suitable for sheepskin.

The most basic image segmentation method is the edge-based detection method,[3] and its core is to convolute the image with the help of differential operators. Common differential operators include Sobel, Roberts, Canny, Laplace operators, etc.[4,5] This kind of method is easy to understand, fast in operation and simple in algorithm implementation, but the edge of detection is often piecewise discontinuous and has poor anti-noise ability. Gray threshold segmentation has been widely studied and applied for its simple, effective and easy to understand characteristics. The threshold algorithm proposed by Otsu et al.[6] is most widely used because of its simple algorithm, real-time performance and strong robustness.[7–9] However, it has poor segmentation effect for images with a lot of noise. A large number of researchers have improved the Otsu algorithm. Chung et al. proposed an acceleration algorithm based on heap and quantization to improve the algorithm efficiency.[10] Liu, Jianzhuang et al. added neighborhood mean to promote Otsu in two dimensions, which improved its anti-noise performance.[11] Jing Xiaojun et al. added neighborhood mean and neighborhood value to promote Otsu in three dimensions and further improved its anti-noise performance.[12] Xu Xiangyang et al. proved that the optimal threshold value found by Otsu method was biased towards the party with greater inter-class variance, and proposed that the method of Otsu was used again for the party with greater variance.[13] For the image with bright target and large difference from the background variance, the segmentation effect was better. Wu Fenghe et al. used an iterative method to find the segmentation threshold and used mathematical morphology for edge connection and defect repair. Realize single-pixel edge segmentation, but for multi-pixel edges, a larger area of mis-segmentation will occur.[14] Since sheepskin pictures have large areas of blood spots and creases, and contain a small amount of salt, the use of the above algorithms to process sheepskin pictures has certain limitations.

*Corresponding author email: 1073547828@qq.com
Manuscript received October 7, 2020, accepted for publication March11, 2021.

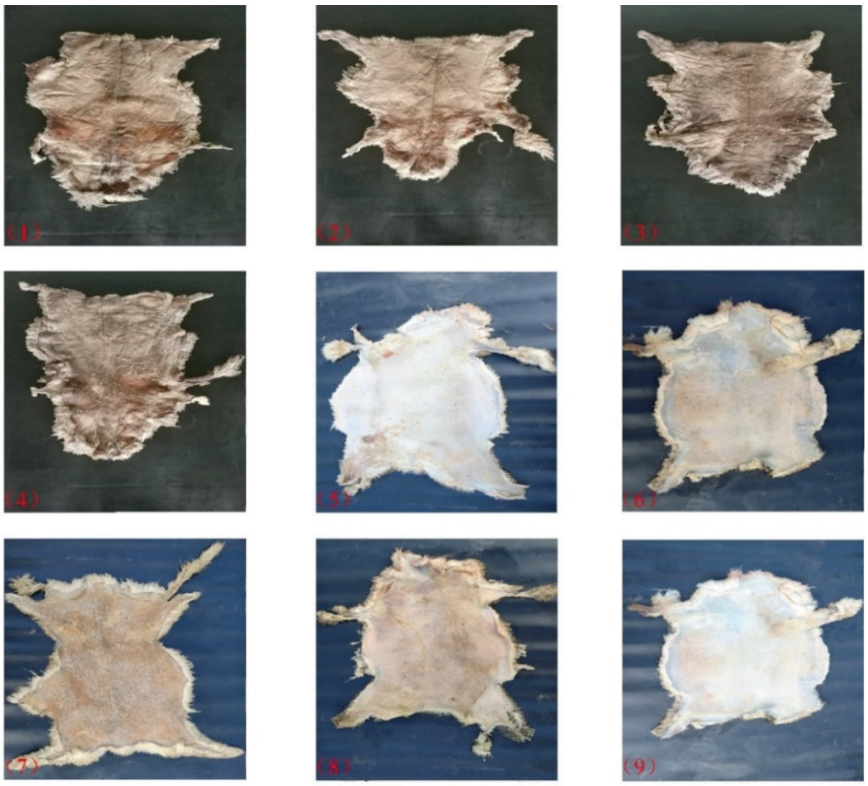

Figure 1. The typical sheepskin pictures collected

According to the characteristics of the collected sheepskin images and computer vision measurement technology, a practical sheepskin contour extraction method based on Otsu and morphology was proposed in this paper, which realized the accurate extraction of the sheepskin contours in raw sheepskin images and provided a theoretical basis for the automation of sheepskin cutting. The method mainly includes four specific steps: (1) The image is preprocessed by pixel-level 3d de-noising system. (2) Binary image segmentation was performed using the fast Otsu threshold algorithm based on image block pixel set. (3) Edge defect filling was performed by morphological treatment. (4) The boundary contour extraction algorithm with topological structure analysis and area threshold algorithm were used to search and extract the contours of the repaired binary images.

Materials and methods

The sampling place of this experiment is a sheepskin manufacturing enterprise in Hebei province. It uses industrial cameras to capture images in indoor natural environments. The sheepskin is placed flat on the conveyor belt. To ensure the reliability of the experiment, a total of 200 different sheepskin pictures were collected in JPG format. The typical sheepskin pictures collected are shown in Figure1.

A preprocessing system based on pixel level 3D de-noising model

Image preprocessing plays an important role in subsequent image processing and can improve image quality. As the first step of image processing, gray transformation is generally used to transform RGB image into gray image.

Sheepskin images collected by camera under natural lighting environment often have some noise due to the vibration of the shooting and cutting platform and the instability of the electrical signal. Secondly, in order to facilitate the storage of raw sheepskin, salt should be sprinkled on the back of the whole piece of sheepskin to prevent the destruction of the sheepskin. The presence of salt also brings interference to the image processing. Common methods to deal with image noise include mean filtering, Gaussian filtering (weighted mean filtering) and median filtering.[15] General de-noising process is on the whole image pixel convolution, then using convolution operator to deal with each pixel, can achieve a certain amount of noise reduction effect, but if to deal with all the pixels that will obscure the details of the image feature and edge points, and the fuzzy degree is proportional to the radius of neighborhood size.[16] In order to achieve the best de-noising effect without destroying details and preserving edge features, a selective de-noising model is proposed.

The selective de-noising model is a three-dimensional grayscale correction model based on the pixel level. The mean value and median value of the field are used to correct the pixel grayscale value, and the size relation among the three is used as the segment judgment mechanism to judge, so as to remove the noise points and bright spots of the pre-processed grayscale image and retain the edges that are easy to be processed into noise.

Assuming an image size is M*N, use $f(x \cdot y)$ to represent the value of the pixel, and $g(x \cdot y)$ to represent the neighborhood mean of the pixel. Use Equation (1) to find the average value of the pixel's neighborhood, Equation (1) is as follows:

$$g(x \cdot y) = \frac{1}{c} \sum_{f \in s} f(x \cdot y) \tag{1}$$

where, c is the number of pixels in the neighborhood, and s is the 3*3 region in the neighborhood. The neighborhood value $h(x \cdot y)$ of the pixel point is:

$$h(x \cdot y) = median\left[\sum_{f \in s} f(x \cdot y)\right] \tag{2}$$

where, median is the operation with a median. According to the pixel gray value, the mean value of neighborhood, and the distance relation between neighborhood values, the relation is:

$$\begin{aligned} |f(x,y) - g(x,y)| > |h(x,y) - g(x,y)| \&\& \\ |f(x,y) - h(x,y)| > |h(x,y) - g(x,y)| \end{aligned} \tag{3}$$

Equation (4) is used to correct the pixel gray value, as shown in Equation (4):

$$f(x,y) = (g(x,y) + h(x,y))/2 \tag{4}$$

When pixel gray value, neighborhood mean, neighborhood value and global average gray value are related as follows:

$$\begin{aligned} |h(x,y) - g(x,y) > |f(x,y) - g(x,y)| \&\& \\ |f(x,y) - h(x,y)| > |f(x,y) - g(x,y)| \&\& \\ avr(src) > f(x,y) \end{aligned} \tag{5}$$

where, $avr(src)$ is the average value of grayscale images. The pixel gray value is corrected to:

$$f(x,y) = h(x,y) \tag{6}$$

In other cases, gray levels are not corrected.

Fast Otsu's threshold segmentation algorithm based on the idea of pixel set

Sheepskin images mainly include foreground and background pixels, and the segmentation needs to meet real-time performance. Therefore, the single threshold segmentation method based on Otsu's idea is used to perform binary segmentation on the image. The basic idea is to traverse all gray levels and search for the maximum variance between classes to find the optimal threshold, the function of variance between classes is:

$$G(t) = \omega_0(t)\left[\mu_T - \mu_0(t)\right]^2 + \omega_1(t)\left[\mu_T - \mu_1(t)\right]^2 \tag{7}$$

where, $\omega_0(t)$ is the sum of the background probability, μ_T is the average intensity of the whole image, $\mu_0(t)$ is the background variance, $\omega_1(t)$ is the sum of the foreground probability, and $\mu_1(t)$is the foreground variance. When $G(t)$ takes the maximum value, the optimal threshold (t^*) is obtained,

$$t^* = \arg\left\{\max_{0 \le t \le L-1} G(t)\right\} \tag{8}$$

where, t is the gray level, L is the maximum gray level. The final binary image is calculated according to the following Equation:

$$f(x,y) = \begin{cases} 1, & f(x,y) > t^* \\ 0, & f(x,y) \le t^* \end{cases} \tag{9}$$

According to xu Xiangyang's proof in the literature, the optimal threshold selected by Otsu algorithm will be biased to the side with greater variance.[13] For the collected sheepskin pictures, the variance of the foreground is far greater than the variance of the background. The threshold value obtained directly by Otsu algorithm will be biased towards the bright foreground, and a small amount of dark sheepskin with blood will be processed into the background, resulting in false segmentation. At the same time, for sheepskin images with a large degree of distinction between the background and the foreground, traversing all gray levels will cause a waste of computing power. Therefore, an image segmentation optimization threshold method and an accelerated search threshold strategy are proposed.

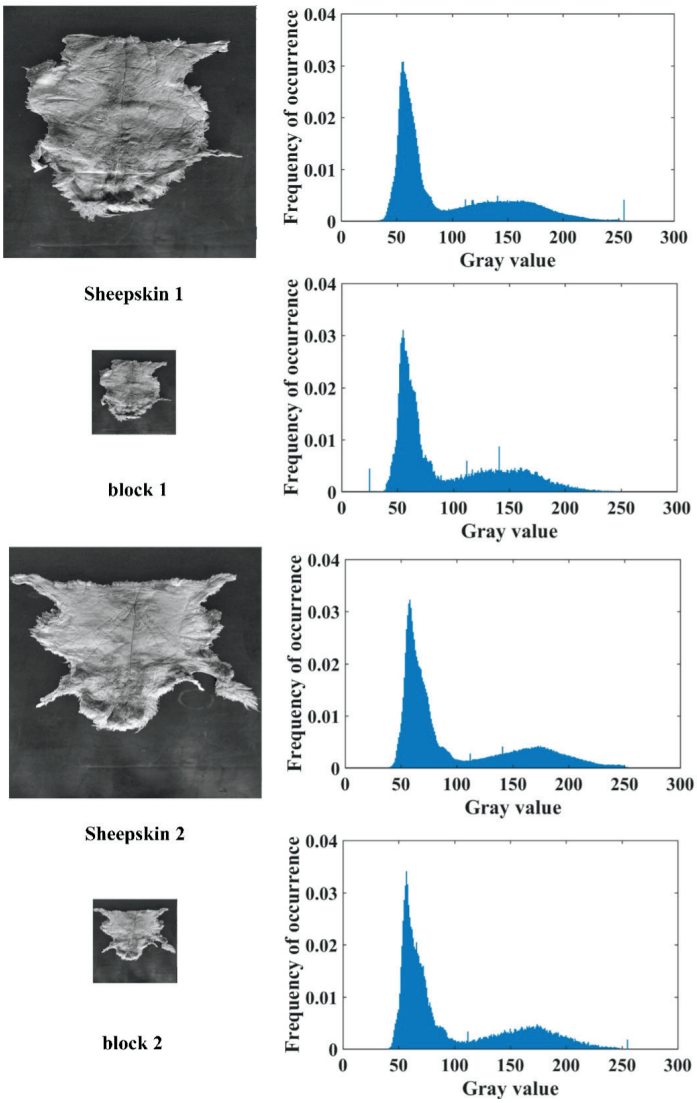

Figure 2. Comparison of gray histogram before and after processing

Image segmentation optimization threshold method

Combining with the threshold bias theory of Otsu's selection demonstrated by Xu Xiangyang, the idea of image segmentation can be used to moderately reduce the variance of the target, and the optimization of the selected threshold can be achieved. The idea of image segmentation is mainly to gather the pixels in the segmentation into a new pixel by averaging or median, forming a new image for threshold selection. This process can effectively reduce the overall variance of the target, help reduce the Otsu selection threshold, and also reduce the image pixels to improve the segmentation speed.

Take k*k pixels in a grayscale image with M×N and grayscale level L as a whole. Calculate the average gray value of the overall pixels of each divided image block and use the average gray value as the new gray value of the pixel block. Use Equation (10) to find the average value of the pixel as the new value of the pixel block. Equation (10) is as follows:

$$F(x \cdot y) = \frac{1}{k * k} \sum_{f \in s} f(x \cdot y) \tag{10}$$

where, $F(x \cdot y)$ is the pixel value of the new image. Then all of the pixel blocks are stored as a whole in a new image whose size is 1/k2 times the original size. (K value is set to 3 for analysis purposes).

The gray histogram comparison of sheepskin before and after partitioning is shown in Figure 2. As can be seen from this figure, the gray histogram before and after partitioning is in a similar bimorphic form as a whole. However, after partitioning, the target area is obviously concentrated and tends to be closer to the background, which can reduce the target variance to a certain extent. This process makes the threshold value obtained by Otsu move towards the background and become lower than before the partition, which is conducive to the expression of the target contour. In order to more visually see the threshold changes before and after image partitioning, the sheepskin in Figure 1 was taken as the experimental object, and the Otsu method was used directly to compare the threshold values obtained after image partitioning, as shown in Figure 3.

Accelerated search threshold strategy

In the Otsu method, for each gray level 0≤t≤L-1, G(t) needs to be calculated once, and finally the G(t) value is compared, and the t value when the value reaches the maximum is selected as the segmentation threshold. The acceleration strategy first calculates the average gray value of the entire image for the obtained gray image and calculates the average value of the gray image with equation 11:

$$arv = t = \frac{K * K}{M * N} \sum_{F \in s} F(x \cdot y) \tag{11}$$

where, *arv* is the average gray average of the image. Using the mean value t of the gray image as the segmentation threshold of the background S0 and the target S1, find their respective mean and variance $\mu_0(t)$, $\mu_1(t)$, $\sigma_0^2(t)$, $\sigma_1^2(t)$. When the maximum inter-variance $G(t)$ was taken, the optimal threshold (t^*) was obtained. Because the background and foreground of sheepskin image were relatively clear, $\mu_0(t)$ and $\mu_1(t)$ had a large difference, which could be used as the upper and lower limits of the threshold search. Value ranges from $\mu_0(t)$ to $\mu_1(t)$, no longer traversing every gray level, greatly improving the search speed. The search equation is as follows:

$$t^* = arg\left\{\max_{\mu_0(t) \le t \le \mu_1(t)} G(t)\right\} \tag{12}$$

Image segmentation algorithm flow

1) Use industrial cameras to collect images on site.

2) Conduct grayscale processing on the collected original images to obtain grayscale images.

3) The grayscale image is denoised robustly by the grayscale correction algorithm in this paper. Equations (1) and (2) are used to calculate the neighborhood value and the mean value. Equations (4), (6) are used to correct grayscale images.

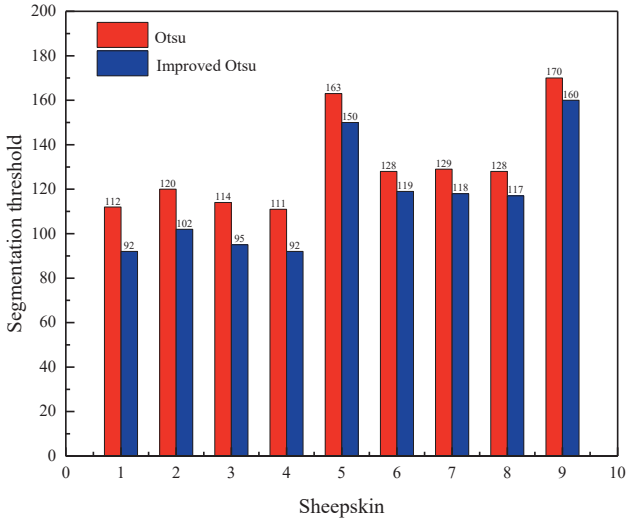

Figure 3. The threshold value obtained by using Otsu method and the improved Otsu method

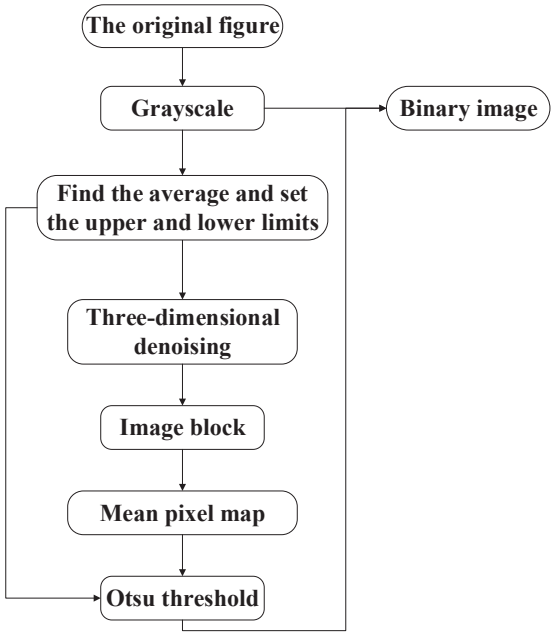

Figure 4. The process of de-noising and threshold segmentation

4) Based on the idea of pixel set, the region mean of the corrected image is calculated by Equation (10), and the pixel value obtained is stored in the new image. The grayscale mean of the whole image obtained by Equation (11) is used as the initial segmentation threshold to divide the image into two categories. The calculated mean value of each category of pixels serves as the upper and lower limit of the threshold value search. Equation (7) was used to calculate the inter-class variance of the gray level between upper and lower limits, and the optimal threshold was searched by comparison.

5) Use the optimal threshold obtained by Otsu algorithm to perform binary segmentation of the corrected grayscale image by Equation (9) to obtain the binary image.

The process of de-noising and threshold segmentation is shown in Figure 3.

Morphological defect repair

Due to the image characteristics and the influence of image noise, the binary image after threshold segmentation is likely to have defects such as rough edges, internal and external holes, broken lines, etc., which will bring difficulties to further contour extraction and further affect the subsequent cutting work. Therefore, effective measures should be taken to eliminate the defects.

Morphological operations are a series of image processing operations based on shapes, which mainly have the functions of dividing independent image elements and connecting adjacent elements. Based on this feature, morphological operations are also selected to deal with these defects.[17,18] Basic operations include: corrosion and expansion of binary or gray values, open and close operations of binary or gray values, morphological gradient, top-hat transformation, etc.

Expansion of A by B means that the structural element B moves from the origin in the Z^2 plane, and "or" operation is performed with the binary image covered by it. The set of expansion images of Point z obtained is as follows:

$$A \oplus B = \{ z \mid (B)_z \cap A \neq \phi \} \tag{13}$$

where, A is the calculated binary image, B is structural element, and $\oplus$ is the expansion operation. A corroded by B represents the set of all z points after "and" operation of structural elements and the covered image, namely:

$$A \Theta B = \{ z \mid (B)_z \in A \} \tag{14}$$

where, Θ is the corrosion operation. B performs the closed operation on A, denoted as $A \bullet B$, namely:

$$A \bullet B = (A \oplus B) \Theta B \tag{15}$$

where, $\bullet$ is a closed operation.

The closed operation eliminates small holes, connects short intervals, and connects adjacent objects.[14] Based on the characteristics of sheepskin images, the selected morphological closure operation can make the detected sheepskin edges smooth, bridge the narrow discontinuity points, and also remove the isolated elements inside.

Contour Extraction

The sheepskin contour extracted using the above-mentioned techniques still has defects, such as internal holes and external noise areas. According to the characteristics of sheepskin contour, the boundary contour tracking technology based on topological structure analysis and the area threshold method are used to extract the outer contour of the sheepskin from the binary image, and the boundary form of the vector is stored. The main principle is to traverse the entire picture in an orderly manner, mark all outer boundaries, hole boundaries and their hierarchical relationships in the image; extract all outer boundaries, discard all hole boundaries; calculate the area of all outer contours, set one contour area threshold, exclude the interference area, and finally the outer boundary contour of the sheepskin is extracted; it is stored in the form of the boundary of the vector point.

Boundary contour tracking technology

Boundary tracking is one of the basic techniques in digital binary image processing and has been studied in depth. Satoshi Suzuki et al. proposed a boundary tracking algorithm with certain topological analysis capabilities. The algorithm extracts the topological structure of the image with less workload and extracts the surrounding

relationship between two types of boundaries: external boundary and hole boundary. This algorithm is the most widely used and efficient, so it is used to extract the target contour. Based on the traditional boundary tracking algorithm, this algorithm uses the idea of coding to assign different integer values to different boundaries. At the same time, the process of obtaining the parent boundary along the boundary is added to determine the outer boundary, hole boundary, and the hierarchical relationship.

The input binary image is the image of 0 and 1, and the pixel value of the image is represented by f(i, j). The raster scan starts from the upper right corner of the image, and the raster scan is interrupted in the following two situations:

$$f(i,j-1)=0, f(i,j)=1 \tag{16}$$

where, f(i, j-1) is the left pixel.

$$f(i,j)\geq 1, f(i,j+1)=0 \tag{17}$$

Boundary tracking is performed on the starting point of the outer boundary of the pixel (i, j) or the starting point of the hole boundary respectively. Here a unique identifier is assigned to the newly discovered boundary, called NBD. Initially, NBD=1, add 1 each time a new boundary is found. Follow the found border from the starting point and mark pixels on the border. The marking strategy is as follows:(a) If the current next boundary is between the 0 component of the pixel (i, j + 1) and the 1 component of the pixel (i, j), please change the value of the pixel (i, j) to NBD. (b) Otherwise, unless (i, j) is on the already followed boundary, set the value of pixel (i, j) to NBD.

Conditions (a) and (b) respectively prohibit the pixel (p, g) from becoming the boundary after the starting point of the hole boundary and the outer boundary that have been followed. After tracking and marking the entire boundary, the raster scan is resumed. When the scan reaches the lower right corner of the picture, the algorithm stops.

Target contour extraction

After the binary image is converted to the boundary representation, only the outer boundary is retained, and the inner hole boundary is discarded. In this way, all the outer boundaries of the binary image are extracted. Next, the area of each contour is calculated, and an area threshold is set at the same time. The area threshold can be set to be less than half of the pixel area of the sheepskin image, and the contour larger than the threshold is retained as the target contour, which is stored in the image matrix in the form of the boundary of the vector point.

Experimental results and analysis

Experimental hardware environment: Inter Core i5 CPU 2.3 GHz, RAM 8GB, Windows 10 64-bit operating system. The programming environment is Open CV2.4.7 + Visual Studio 2010.

Effect analysis of contour extraction method

In this experiment, the sheepskin pictures collected on site are simulated and verified. In order to more clearly analyze the processing effect of the contour extraction algorithm proposed in this paper and understand the role of each link, three methods are added for comparative analysis with the method in this paper. To facilitate observation and comparison, each method uses the

Figure 5. Segmentation effect comparison of four methods

result after contour tracking processing. The three methods are the Otsu segmentation method without morphological processing, the Otsu segmentation method with morphological processing and the improved Otsu segmentation method without morphological processing. Four methods were used to process the collected sheepskin images, and the results of the three image segmentation methods were compared with the methods presented in this paper, as shown in Figure 5.

By comparing the two groups of sheepskin pictures (b), (d) or (c) and (e) in Figure 5, it can be observed that the higher threshold treated some darker sheepskin with blood into the background, with poor edge retention. Algorithm in this paper the threshold is lower than traditional Otsu algorithm, because the sheepskin compared with background brighter, lower threshold will make dark speck to effectively express, also on sheepskin outside of the image contour recognition more accurate, effective protection of the edge information, to obtain a relatively complete sheepskin outer contour, is advantageous to the subsequent cutting processing.

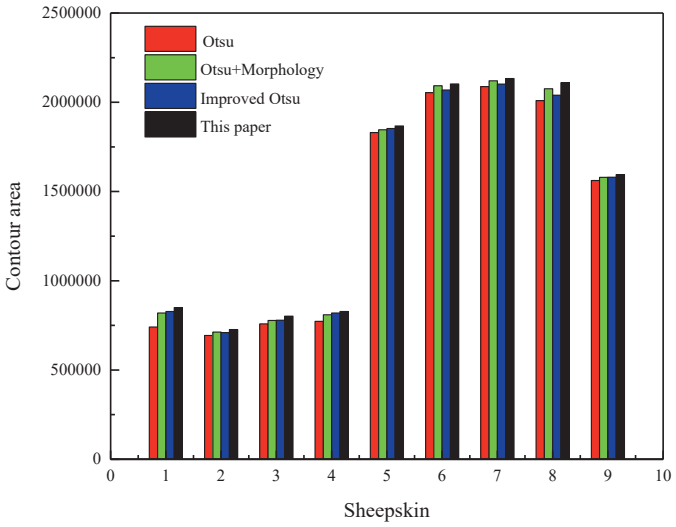

Figure 6. The comparison of contour area obtained by the four methods

By comparing the two groups of sheepskin pictures (b), (c) or (d) and (e) in Figure 5, it can be observed that there are more broken edges in sheepskin edges without morphological treatment, and the extracted contour edges are incomplete and have large errors. After adding morphological treatment, the edges containing defects were connected to obtain a complete sheepskin contour.

In general, the contour method proposed in this paper can extract relatively accurate sheepskin contour. In order to quantitatively analyze the extraction precision of sheepskin contour, the area of contour extracted by the four methods mentioned above was calculated. The comparison of contour area obtained by the four methods is shown in Figure 6. It can be seen from Figure 6 that whether the traditional Otsu is improved or morphological defect processing is added, false segmentation can be effectively reduced. In contrast, the improved Otsu segmentation algorithm has a slightly greater impact on contour extraction than morphological post-processing.

Comparison and analysis of pre-treatment de-noising effect

In order to verify the denoising effect of the model, different levels of Gaussian and salt-and-pepper noise were added to the sheepskin images, and then gray scale correction was carried out under the model. In this experiment, several groups of noise variables are set, and the Gaussian noise levels are σ=0.3, σ=0.5 and σ=1. Salt and pepper noise densities are 10000 and 100000. The final noise diagram and processing results are shown in Figure 7.

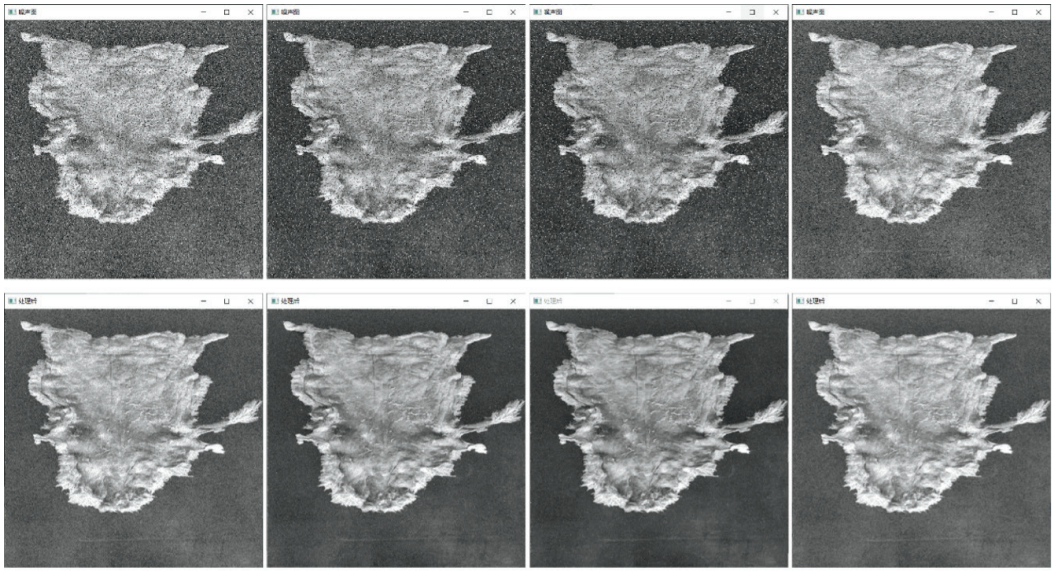

Figure 7. The algorithm in this paper processes the results of noisy graphs

As shown in Figure 8, the denoising algorithm proposed in this paper has a good filtering effect on general additive noise and random noise, and at the same time, it plays a certain smoothing effect on the image and has excellent edge protection. Especially for the removal of salt and pepper noise has intuitive removal effect.

To objectively evaluate the effectiveness of the algorithm proposed in this paper, 3*3 mean filter, Gaussian filter and median filter were used to process the sheepskin original image of the above experiment, and three evaluation indexes relatively recognized by the industry were used to evaluate and analyze the filtering effect.

The evaluation indexes are as follows: Mean Square Error (MSE) refers to the expected value of the square of the difference between the image to be evaluated and the original image, and the smaller the value is, the better the image recovery will be. Peak signal-to-noise ratio (PSNR) is the ratio of the energy of the peak signal to the average energy of the noise. The greater the value, the better. Structural similarity (SSIM) is also a full reference image quality evaluation index. It measures the similarity of two images from brightness L(x,y), contrast C(x,y) and structure S(x,y). The larger the value is, the better, and the maximum value is 1. The evaluation values were recorded in Table I.

It can be seen from Table I that the method in this paper has the highest structural similarity, the peak signal-to-noise ratio and the lowest mean square deviation. The low mean square error indicates that the image distortion is the least after the proposed algorithm is used. The larger PSNR indicates that the proposed algorithm has the best denoising ability. The structural similarity between the Gaussian filter and the proposed algorithm is large, which indicates that the mean filter and the median filter sacrifice the detail of the image in order to achieve the ability of image denoising. It also indicates that the detail and edge protection performance of the proposed algorithm are better than other filters. All the numerical results show that the method presented in this paper is the best for sheepskin image processing. These three kinds of evaluation systems can show that the method proposed in this paper has scientific effectiveness and applicability.

Force analysis of image segmentation algorithm

The experimental subjects are mainly sheepskin images with pixel sizes of 1080×1920, 2457×1627 and 2589×1846, etc. The proposed segmentation algorithm was compared with Otsu and 2-D Otsu algorithms. The Otsu and 2-D Otsu algorithms are matched with the algorithms in this paper, such as Table II. The calculation time of Otsu algorithm is at the level of 100ms, while that of 2-D Otsu algorithm is about 4.5 times that of Otsu. The speed of this algorithm in processing sheepskin images is improved by 170% and 1080% compared with the traditional Otsu algorithm. It greatly improves the efficiency of the algorithm and meets the real-time requirement of industrial field cutting.

Conclusion

The use of computer vision measurement technology to realize the automatic cutting of the edging has changed the work mode of the company's manual cleaning of the edging. It solves the problem of labor intensity caused by high labor intensity and poor working environment in enterprise production and processing, and at the same time improves production efficiency and optimizes costs. The sheepskin contour extraction method proposed in this paper has a pixel-level three-dimensional denoising preprocessing system, uses a fast Otsu threshold algorithm based on image block pixel sets to segment binary images, uses morphological processing to fill edge defects, and using the boundary contour tracking algorithm based on topology analysis to extract the contour information, the largest the algorithm for sheepskin image processing effect is better. The 3d selective noise reduction model overcomes the noise interference caused by salt and effectively protects the sheepskin edge. Compared with the traditional one-

Table I

The evaluation values

Evaluation method	Average filtering	Gaussian filter	Median filtering	This paper
MSE	7.98101	4.75446	4.07791	3.30345
PSNR	39.1102	41.3598	42.0264	42.9411
SSIM	0.325682	0.32858	0.32766	0.328812

Table II

Comparison of the efficiency of Otsu 2D-Otsu and this paper (ms)

Sheepskin	Otsu	2D-Otsu	This paper	Faster than Otsu	Faster than 2D-Otsu
1	132.8	591.6	52.4	153%	1029%
2	141.3	611.4	54.3	160%	1026%
3	140.6	594.5	51.0	176%	1066%
4	139.4	580.0	55.1	153%	953%
5	257.1	1226.7	89.5	187%	1271%
6	331.7	1277.4	109.0	204%	1072%
7	269.4	1276.8	118.0	128%	982%
8	312.5	1273.4	108.5	188%	1074%
9	257.1	1218.1	90.5	184%	1246%
Average				170%	1080%

dimensional Otsu algorithm, the fast Otsu threshold segmentation technology of image block pixel set improves the processing rate by nearly 160%, meeting the real-time demand of industrial cutting. At the same time, the edge positioning is more accurate, and the outer contour with more complete and larger area is obtained with lower threshold, which reduces the mis-segmentation by nearly 3%. Morphological processing is used to fill in edge defects, and the boundary contour tracking algorithm of topological structure analysis obtains complete and accurate outer edge information. The sheepskin contour extraction method can obtain the accurate sheepskin contour information which can be operated by the cutting platform, which provides the theoretical basis for the sheepskin image cutting and a solid step for the realization of automatic sheepskin cutting. The algorithm presented in this paper is also suitable for the segmentation of other simple images with clear target and background and bright target, so it has a certain application prospect.

Acknowledgments

The authors gratefully acknowledge the fund of Shaanxi University of Science and Technology (BJ15-19), and the Youth Innovation Team of Shaanxi Universities.

References

1. Zhang, B.; Principles, developments and applications of computer vision for external quality inspection of fruits and vegetables: A review. Food Research International **62**, 326–343, 2014.
2. Wäldchen, J., Mäder, P.; Plant Species Identification Using Computer Vision Techniques: A Systematic Literature Review. Arch. Comput. Methods Eng. **25**, 507–543, 2018.
3. Ferandji, Y.G., Diaraya, Lawi, A.; Performance Comparison of Image Edge Detection Operators for Lontara Sanskrit Scripts. 2nd East Indonesia Conference on Computer and Information Technology, pp. 241–244, 2018.
4. Ganesan, P. and Sajiv, G.; A comprehensive study of edge detection for image processing applications. International Conference on Innovations in Information. Embedded and Communication Systems, pp. 1–6, 2017.
5. Yousaf, R. M., Habib, H. A., Dawood, H. and Shafiq, S.; A comparative study of various edge detection methods. 14th International Conference on Computational Intelligence and Security, pp. 96–99, 2018.
6. Otsu, N.; A Threshold Selection Method From Gray-Level Histograms. IEEE Transactions on Systems Man & Cybernetics C(**1**), 62–66, 1979.
7. Mizushima, A., Lu, R.; An image segmentation method for apple sorting and grading using support vector machine and Otsu's method. Computers and Electronics in Agriculture **94**, 29–37, 2013.
8. Talab, A. M. A., Huang, Z., Xi, F and Haiming, L.; Detection crack in image using Otsu method and multiple filtering in image processing techniques. Optik 127(**3**), 1030–1033, 2016.
9. Goh, T. Y., Basah, S. N., Yazid, H., Aziz Safar M. J., and Ahmad Saad F. S.; Performance analysis of image thresholding: Otsu technique. Measurement **114**, 298–307, 2018.
10. Chung, K. L., Tsai, C. L.; Fast incremental algorithm for speeding up the computation of binarization. Applied Mathematics and Computation 212(**2**), 396–408, 2009.

11. Liu, J., Li, W., Tian, Y.; Automatic thresholding of gray-level pictures using two-dimensional Otsu method. Acta Automatica Sinica 19(**1**), 101–105, 1993.
12. Jing, X. J., Li, J. F., Liu, Y. L.; Image segmentation based on 3-D maximum between-cluster variance. Acta Electronica Sinica 31(**9**), 1281–1285, 2003.
13. Xu, X., Xu, S., Jin, L., Song, E.; Characteristic analysis of Otsu threshold and its applications. Pattern Recognition Letters 32 (**7**), 956–961, 2011.
14. Wu, F. H.; A study on contour extraction method in computer vision measurement technology. Acta Metrologica Sinica 28(1), 18–22, 2007.
15. Kumar, V., Yadav, P., Samadhiya, A., Jain, S and Tiwari, P.; Comparative Performance Analysis of Image De-noising Techniques. International Conference on Innovations in Engineering and Technology, pp. 47–52, 2014.
16. Zhu, Y., Huang, C.; An Improved Median Filtering Algorithm for Image Noise Reduction, Physics Procedia **25**, 609–616, 2012.
17. Zhao,Y. Q., Gui, W. H., Chen, Z. C., Tang, J. T and Li, L. Y.; Medical Images Edge Detection Based on Mathematical Morphology, International Conference of the Engineering in Medicine & Biology Society, pp. 6492–6495, 2005.
18. Dufour A.; Filtering and segmentation of 3D angiographic data: Advances based on mathematical morphology, Medical Image Analysis **17**, 147–164,2013.

Tanning Performance of a Novel Chrome-Free Complex Tanning Agent: Penetration and Distribution

by

Zhen Wang,[1] Ya-nan Wang,[1,2,*] Yue Yu[1,*] and Bi Shi[1,2]

[1]*National Engineering Research Center of Clean Technology in Leather Industry, Sichuan University,* Chengdu 610065, China

[2]*Key Laboratory of Leather Chemistry and Engineering of Ministry of Education, Sichuan University,* Chengdu 610065, China

Abstract

Penetration of tanning agent in leather plays an important role in tanning performance and properties of finished leather. A novel complex tanning agent composed of Al–Zr salts and highly-oxidized starch ligand, named TWLZ, was used for chrome-free tanning. The masking effect of highly-oxidized starch reduced the electropositivity of metal complexes, which should help penetration of TWLZ and moderate its fixation during tanning. The effects of tanning agent dosage, basification method and pretreatment method on the distribution of TWLZ in leather were investigated. Using 8% TWLZ and basifying with magnesium oxide benefited the penetration and distribution of TWLZ throughout the cross-section of leather. Pretreatment with an amphoteric organic tanning agent could regulate the charge state of the hide, balance the penetration and fixation of TWLZ, and thus show uniform distribution and satisfactory tanning performance. This work will guide the establishment of TWLZ chrome-free tanning system.

Introduction

Reducing chrome input in leather production is the current consensus and an inevitable trend to achieve the sustainable development of the leather industry.[1-3] Therefore, numerous chrome-free tanning technologies have been developed as possible alternatives to the prevailing chrome tanning.[4-6] Among these technologies, non-chrome mineral tanning, such as aluminum and zirconium tannage, are still considered a promising substitute to chrome tanning.[7,8] This is because the tanned leather shows a similar dehydrated state and charge property (high isoelectric point) to wet blue and matches well with the current post-tanning processes.[9] However, traditional aluminum tanning gives leather with good softness, but poor stability to heating and washing.[10] Zirconium salts have good filling properties, however its strong binding ability with skin collagen will make leather firm and rigid.[11] One of the main reasons is attributed to the high hydrolysis and olation ability of Al/Zr salts,[10,11] thereby leading to the deposition and overload of Al/Zr salts on the surface of leather.[12,13] Therefore, an essential issue involved in the application of non-chrome mineral tanning agents is to resolve the conflict between penetration and fixation and achieve a uniform distribution of the tanning agent.

A useful approach to moderate fixation and promote penetration of Al/Zr salts is the introduction of a masking agent (ligand) into the metal complex.[14] The use of some micromolecular organic acids, such as lactic acid and citric acid, is familiar to tanners.[15,16] Unfortunately, the upgrade on distribution uniformity of metal salts was not significant according to previous work.[13] We recently developed a novel chrome-free complex tanning agent where a highly oxidized starch ligand was introduced into an Al–Zr bimetal complex and resulted in excellent tanning performance.[9,17] This ligand is supposed to show good masking performance due to its multiple carboxyl groups and relatively large molecular size, and thus may favor the penetration and distribution of Al–Zr complexes. This tanning agent containing Al–Zr salts and the starch ligand was named as TWLZ. In this study, the charge property of TWLZ was determined to elucidate the mechanism of penetration and fixation of TWLZ in leather. Furthermore, the effects of tanning agent dosage, basification method and pretreatment method on TWLZ distribution were investigated to formulate an optimal recipe for uniform distribution of TWLZ. Our aim was to develop a practical tanning technology and provide a basis for the industrial application of TWLZ in a chrome-free tanning system.

Experimental

Materials

Pickled cattle hide was purchased from a local tannery. A powdery chrome-free complex tanning agent named TWLZ was prepared by mixing $Al_2(SO_4)_3{\cdot}18H_2O$ (60 wt%), $Zr(SO_4)_2{\cdot}4H_2O$ (25 wt%), and highly-oxidized starch (15 wt%) according to our previous work.[17] A blend of $Al_2(SO_4)_3{\cdot}18H_2O$ (70.6 wt%) and $Zr(SO_4)_2{\cdot}4H_2O$ (29.4 wt%) was also prepared for determining the charge property of metal complexes. The only difference between this blend and TWLZ was that the highly-oxidized starch ligand was not included in this blend. Three types of pretreatment agents used before tanning, i.e. anionic fatliquoring agent (AFA), cationic fatliquoring agent (CFA), and amphoteric organic tanning agent (TWS), were provided by Tingjiang New Materials Co., Ltd. (Sichuan, China).

Charge property of metal complexes in TWLZ

The contents of cationic, anionic and electroneutral metal complexes in the TWLZ solution were determined using a

* Corresponding authors email: wangyanan@scu.edu.cn; yuyue@scu.edu.cn

Manuscript received February 9, 2021, accepted for publication March 31, 2021.

precipitation method[18] to reveal the charge state of the TWLZ tanning agent in the initial stage of tanning. Twenty ml of 1.5 g/L TWLZ solution was mixed with 1 ml anionic precipitant (Sodium diisobutyl naphthalenesulfonate, a type of anionic surfactant, Xinrunde Chemical Co. Ltd., Hubei, China). This blend was centrifuged for 5 min at a speed of 5000 r/min and washed by distilled water to obtain the precipitate. The precipitate was digested with hydrogen peroxide and nitric acid using a microwave device (Multiwave PRO, Anton Paar, Austria), and its Al and Zr contents were determined by ICP-OES (Optima 8000, PerkinElmer, USA). The sum of Al and Zr contents was defined as the cationic metal complexes content. Similarly, 20 mL of 1.5 g/L TWLZ solution was mixed with 0.05 ml cationic precipitant (a type of cationic polyamine resin, Jogel Industrial Co., Ltd., Shanghai, China) to form a precipitate. Centrifugation, digestion and ICP-OES analysis were followed to obtain the anionic metal complexes content. Al and Zr contents of the TWLZ solution were determined by ICP-OES after direct digestion, and their sum was defined as the total metal complexes content. The cationic metal complexes percentage and anionic metal complexes percentage of TWLZ can be calculated according to formulas (1) and (2). The remaining part was considered as the electroneutral metal complexes percentage.

$$\text{Anionic metal complexes percentage (\%)} = \frac{\text{Anionic metal complexes content}}{\text{Total metal complexes content}} \times 100 \quad (1)$$

$$\text{Cationic metal complexes percentage (\%)} = \frac{\text{Cationic metal complexes content}}{\text{Total metal complexes content}} \times 100 \quad (2)$$

In addition, a blend of $Al_2(SO_4)_3{\cdot}18H_2O$ and $Zr(SO_4)_2{\cdot}4H_2O$ mentioned in Materials was also used for determining the charge property of metal complexes following the same procedures.

Determination of zeta potential of pretreatment agents

CFA emulsion (2 g/L), AFA emulsion (0.5 g/L) and TWS solution (20 g/L) were prepared for Zeta potential determination. The pH of emulsion/solution was adjusted from 2.5 to 6.5 using 0.1 mol/L HCl solution or 0.5 mol/L NaOH solution. The zeta potentials of the samples at different pH values were measured by a particle size & zeta potential analyzer (NanoBrook Omni, Brookhaven, USA).

Effect of TWLZ dosage on distribution of TWLZ in leather

Three pieces of pickled cattle hide (30 cm × 30 cm, from symmetrical parts along the backbone) were tanned using 6%, 8% and 10% TWLZ (based on limed weight, the same below), respectively. The tanning process is shown in Table I. The duration of tanning with TWLZ before basification was defined as a penetration stage. Samples (2 cm × 2 cm) were taken at the end of TWLZ penetration and tanning, and were split into grain layer, middle layer and flesh layer by a freezing microtome to determine the layered contents of the tanning agent. The shrinkage temperature of tanned leather was measured at the end of tanning.

Effect of basification method on distribution of TWLZ in leather

Three pieces of pickled cattle hide (30 cm × 30 cm, from symmetrical parts along the backbone) were tanned with 8% TWLZ separately. The tanning process was based on Table I except that basification operations were conducted differently (see Table II). The final basification pH was controlled at pH 4.0 for all the groups. Samples were taken at the end of basification and tanning to determine the layered contents of the tanning agent.

Effect of pretreatment on distribution of TWLZ in leather

Four pieces of pickled cattle hide (30 cm × 30 cm, from symmetrical parts along the backbone) were tanned according to the recipe shown in Table III. Pretreatment using 2% pretreatment agent (CFA, AFA

Table I

Tanning process

Process	Material	Temperature (°C)	Dosage (%)	Time (min)	Remarks
Tanning	Water		100		
	Sodium chloride		7	15	Drain 20%
	TWLZ		6/8/10	300	Sample and stop overnight. Next day run for 30 min. pH < 2.0
	Magnesium oxide		0.3×3	30×3	
	Sodium bicarbonate		0.5×3	15×3	
	Water	40	200	120	Stop overnight. Next day run for 30 min and sample. pH = 4.0

Table II

Basification operations

Method	Basification operations
Mixed basification	0.3% magnesium oxide was added 3 times at intervals of 30 min. Then 0.5% sodium bicarbonate was added 3 times at intervals of 20 min. Afterwards, the drum kept running for 90 min.
Sodium bicarbonate basification	0.5% sodium bicarbonate was added 3 times at intervals of 15 min, followed by addition of 0.3% sodium bicarbonate for 6 times at intervals of 20 min. Then the drum kept running for 75 min.
Magnesium oxide basification	1.1% magnesium oxide was added, and the drum kept running for 240 min.

Table III

Tanning process with pretreatment

Process	Material	Temperature (°C)	Dosage (%)	Time (min)	Remarks
Pretreatment	Water		100		
	Sodium chloride		7	15	Drain 20%
	Pretreatment agent		2	60	
Tanning	TWLZ		8	300	pH < 2.0
	Magnesium oxide		1.1	240	
	Water	40	200	120	Stop overnight. Next day run for 30 min and sample. pH = 4.0

or TWS) was conducted before TWLZ tanning for 60 min. One piece of hide was directly tanned by 8% TWLZ without pretreatment as the control. The other operations of the control group were the same as Table III. The tanned leathers were sampled for determination of layered contents of tanning agent and isoelectric point.

Determination of tanning agent contents in layered leather

The thickness of leather sample was measured by a thickness gauge. Then the sample was split into three layers with equal thickness, which were grain layer, middle layer and flesh layer, by a freezing microtome (CM1950, Leica, Germany). The split samples were dried to constant weight and digested for determining Al and Zr contents by ICP-OES. The tanning agent contents (the sum of Al_2O_3 and ZrO_2, based on the weight of dry leather) in the three layers were calculated to evaluate the distribution of tanning agent in leather. Measurements were made in triplicate, and the results were presented as the means ± standard deviation. Additionally, the distribution index of tanning agent was calculated as formula (3) according to previous work:[13,16]

$$\text{Distribution index (\%)} = \frac{2 \times M}{G + F} \times 100 \quad (3)$$

where G is the tanning agent content in grain layer, M is the tanning agent content in middle layer, and F is the tanning agent content in flesh layer.

Determination of isoelectric point (pI) of leather

The pI of pickled hide/tanned leather was determined according to literature.[19] In brief, a leather sample was dried and ground into fine fibers using a grinding mill (ZM 200, Retsch, Germany). Then 10 g of the ground sample was dispersed in 400 ml of water to measure the zeta potentials at different pH values by a zeta potential analyzer (Mütek SZP-10, BTG, Germany). The pI of leather, which was the pH value at the zero point of zeta potential, was found from the pH-zeta potential curve.

Results and Discussion

Charge properties of tanning agent, pickled hide and tanned leather

Electrostatic interactions between chemicals and leather are considered one of the driving forces for the mass transfer of chemicals in leather.[9,20,21] Moreover, the coordination reaction between tanning metal ions and carboxyl anions on collagen is related to the charge state of the pickled hide.[19] Thus, the penetration, fixation and distribution of tanning agents in leather should be influenced by the charge properties of both tanning agent and pickled hide. The blend of Al–Zr salts is strongly electropositive in aqueous solutions (Figure 1a) since it is easy to undergo hydrolysis and olation to form cationic complexes.[10,11] This will lead to rapid surface bonding and an uneven

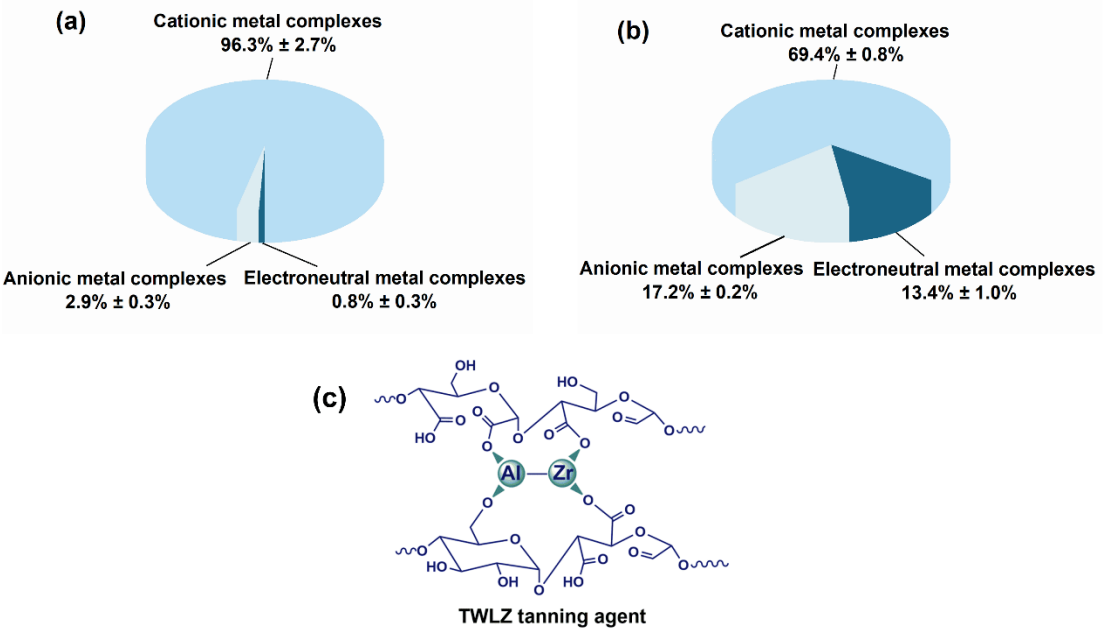

Figure 1. The proportion of metal complexes with different charge states in **(a)** $Al_2(SO_4)_3$–$Zr(SO_4)_2$ blend and **(b)** TWLZ; **(c)** structural schematic diagram of TWLZ.

distribution of Al–Zr salts in leather[13] because its carboxyl anion in collagen attracts cationic metal complexes by electrostatic force and then coordinates with metal ions. Figure 1b shows that cationic metal complexes accounted for only 69.4% of all the components in the TWLZ tanning agent (a blend of aluminum sulfate, zirconium sulfate and highly-oxidized starch), and the proportions of anionic metal complexes and electroneutral metal complexes grew to 17.2% and 13.4%, respectively, compared with the blend of Al–Zr salts. This result should be attributed to the introduction of a highly-oxidized starch, a macromolecular ligand with multiple carboxyl groups, into the metal complexes.[7] The masking effect of the ligand reduced the electropositivity and reactivity of metal complexes (Figure 1c) and should benefit the penetration of metal complexes. Meanwhile, the pI of pickled hide was 5.5 (Figure 2), suggesting that the pickled hide was electropositive, and the ionization of carboxyl groups was restricted in the initial stage of tanning (pH < 2.0). This result was also beneficial to the uniform penetration of metal complexes. As the tanning float pH rose during basification, the electropositivity of metal complexes was enhanced. The carboxyl groups on collagen were gradually ionized to carboxyl anions and participated in the coordination, and thereby resulted in the bonding and crosslinking of cationic metal complexes in leather. This reaction can also be demonstrated by the fact that the pI of tanned leather increased to 7.1 after tanning (Figure 2).

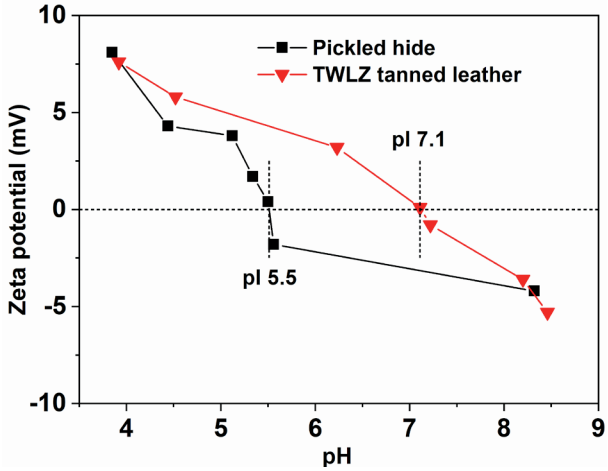

Figure 2. Zeta potentials of pickled hide and TWLZ tanned leather at different pH values.

Effect of TWLZ dosage on distribution of TWLZ in leather

Pickled hide was tanned with 6%, 8% and 10% TWLZ tanning agent, respectively. The tanned leather was split into three layers, i.e. grain, middle and flesh layers, for the determination of tanning agent content. The distribution of the tanning agent in leather after penetration and tanning is shown in Figure 3. A penetration stage was set before basification. Figure 3a shows that TWLZ penetrated into the middle layer at that time, and its distribution uniformity was enhanced with the increase of dosage. This result can be attributed to one of the main driving forces of diffusion, namely the concentration gradient. Basification, increasing float length and raising temperature were conducted afterwards to promote the bonding and fixation of Al–Zr complexes in leather. The tanning agent contents in leather after tanning (Figure 3b) were all higher than those after penetration (Figure 3a) and showed a gradual growth with the increase of TWLZ dosage. This resulted in the enhancement of tanning effects as the shrinkage temperatures of tanned leather were 76.2°C, 81.0°C and 83.1°C when using 6%, 8%, and 10% TWLZ. The distribution uniformity of TWLZ can be evaluated by the standard deviation (SD) of tanning agent contents

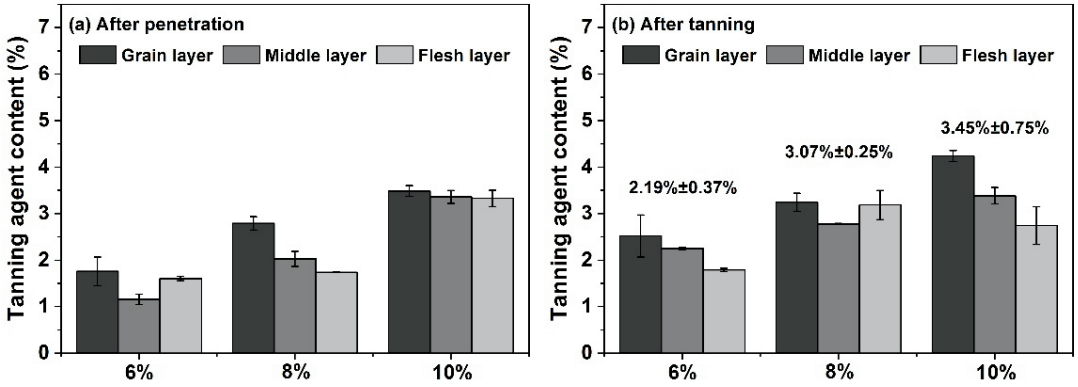

Figure 3. Effect of TWLZ dosage on distribution of TWLZ in leather (**a** after penetration; **b** after tanning)

in grain, middle and flesh layer of the tanned leather. When TWLZ dosage was 8%, the SD of tanning agent contents in the layered leather was lower than the other groups, suggesting more uniform distribution of tanning agent in leather. Further increasing the TWLZ dosage led to the deposition of Al–Zr complexes on grain surface.

Effect of basification method on distribution of TWLZ in Leather

Basification was conducted during the mineral tanning process to get good exhaustion of the metal salts. Inappropriate basification may result in an uneven distribution of the tanning agent, precipitation on leather surface and unsatisfactory properties of finished leather. Here, the effect of basification method on the distribution of TWLZ was investigated. Figure 4 illustrates that basification with magnesium oxide showed higher tanning agent content and a more uniform distribution (lower SD) after tanning compared with the other two basification methods. Magnesium oxide with a low solubility was slowly consumed throughout the tanning process, thereby leading to a continuous pH rise and gradual fixation of tanning agent. Thus, the penetration and binding of TWLZ in leather was more sufficient than the other groups. Sodium bicarbonate basification and mixed basification are batch-type basification. The pH rise fluctuated and showed a zigzag upward trend, particularly at the later stage of tanning. Thus, an uneven distribution of tanning agent was obtained for sodium bicarbonate basification and mixed basification (Figure 4b).

Effect of pretreatment on distribution of TWLZ in leather

In order to improve the penetration, distribution and exhaustion of tanning agents, pretreatment with fatliquors or pretanning agents is commonly carried out before tanning. Here we chose three agents with different charge types for pretreatment. Figure 5 shows that AFA was in an electronegative state in the pH range of 2.5 to 6.5. CFA maintained an electropositive state in the pH range of 2.5 to 6.5. TWS possessed a zwitterionic property with a pI of 4.57. Different pretreatments resulted in quite different tanning performances (Figure 6 and Table IV). As for the distribution uniformity, TWS group performed better in terms of a lower SD of tanning agent contents in layered leather (Figure 6) and a higher distribution index of tanning agent (Table IV) compared with the other groups. On the other hand, AFA group showed the highest SD and the lowest distribution index, indicating an uneven distribution of tanning agent in leather. These results can be explained by the charge state of chemicals/leather and the electrostatic interaction between them. CFA and TWS were electropositive during pretreatment and initial tanning stage (pH < 3). They easily penetrated into the positively

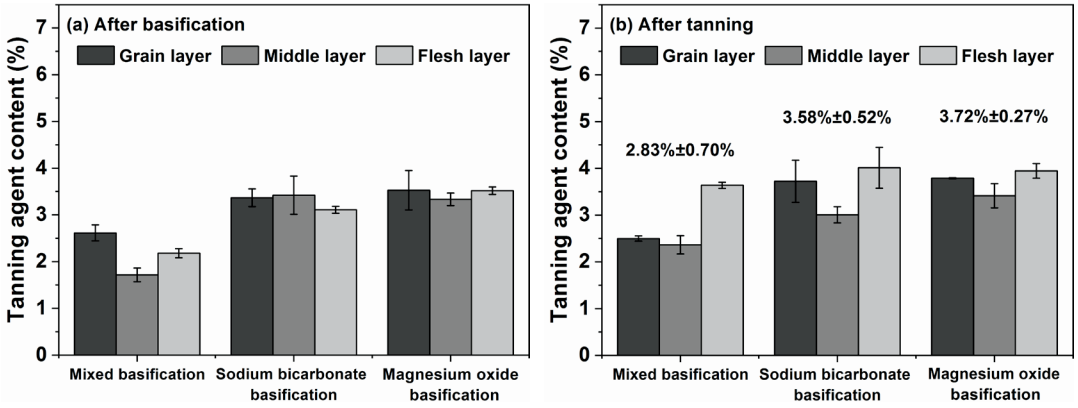

Figure 4. Effect of basification method on distribution of TWLZ in leather (**a** after basification; **b** after tanning)

charged hide by electrostatic repulsion and bound with collagen carboxyl anions, which can be demonstrated by the pI growth of pretreated hide (Figure 7). Therefore, the following coordination of cationic complexes of TWLZ with collagen carboxyl anions was temporarily retarded, and TWLZ tended to penetrate into the core of leather and distribute evenly. In the opposite case, the introduction of anionic AFA reduced the electropositivity of hide (see the pI in Figure 7) and led to excessive surface fixation and uneven distribution of TWLZ.

In addition, CFA group exhibited the lowest total content of tanning agent (3.69%, see Figure 6). This is because of the competitive binding of CFA and TWLZ to leather at the later stage of tanning as they were both cationic chemicals. TWS group showed the highest total content of TWLZ as well as the T_s of leather. The reason should be attributed to the fact that the electropositivity of TWS turned down sharply (Figure 5) as the pH rose during basification, thereby promoting the fixation of TWLZ at the later stage of tanning. As a result, pretreatment with amphoteric agent TWS is beneficial to TWLZ tanning system in consideration of both penetration and fixation of tanning agent.

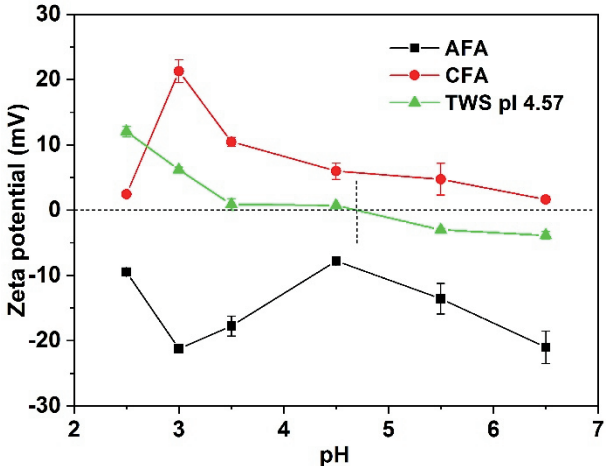

Figure 5. Effect of pH on zeta potential of pretreatment agent.

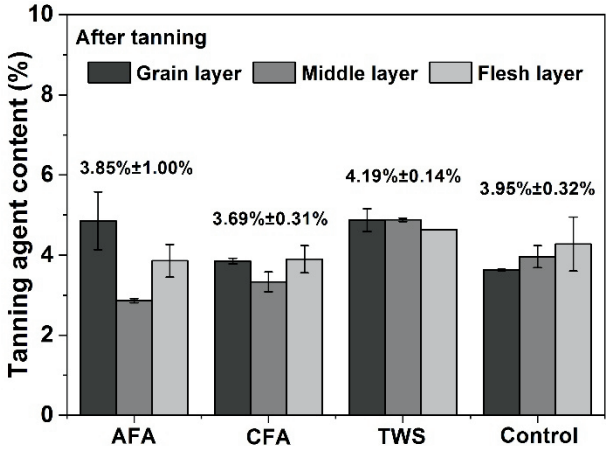

Figure 6. Effect of pretreatment on distribution of TWLZ in leather.

Table IV

Properties of TWLZ tanned leather using different pretreatment methods

Group	T_s (°C)	Distribution index of tanning agent (%)
AFA	79.8 ± 0.2	66.3 ± 8.6
CFA	80.2 ± 0.3	86.2 ± 4.6
TWS	81.9 ± 1.0	102.7 ± 3.1
Control	80.0 ± 0.3	100.6 ± 8.8

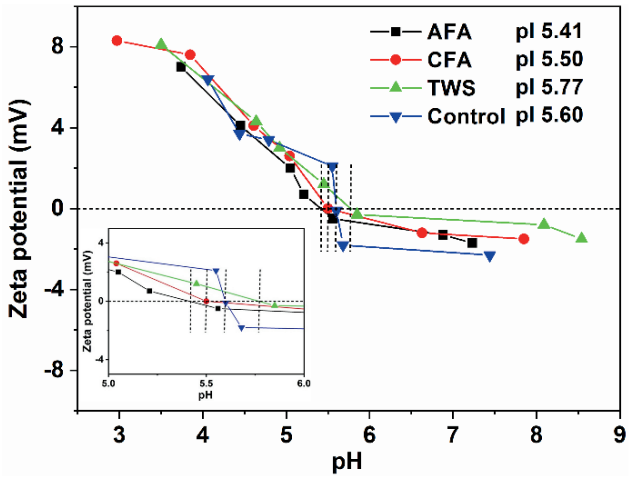

Figure 7. pIs of pretreated hide before tanning.

Conclusions

A complex tanning agent composed of Al–Zr salts and highly-oxidized starch named TWLZ can evenly distribute in the cross-section of leather because the highly-oxidized starch ligand effectively masked the metal ions and reduced the electropositivity of complexes. Using 8% TWLZ, basification with magnesium oxide and pretreatment with an amphoteric organic tanning agent benefited the penetration and uniform distribution of TWLZ in leather. This work is expected to provide a basis for the industrial application of TWLZ in chrome-free tanning system.

Acknowledgement

This work was financially supported by Tianfu Ten-thousand Talents Program of Sichuan Province.

References

1. Wang, Y. N., Shi, B.; Progress of key clean technologies in leather industry. *Chem Ind Eng Prog.* **35**, 1865-1873, 2016.
2. China, C. R., Maguta, M. M., Nyandoro, S. S., Hilonga, A., Kanth, S. V., Njau, K. N.; Alternative tanning technologies and their

suitability in curbing environmental pollution from the leather industry: A comprehensive review. *Chemosphere*, **254**, 126804, 2020.
3. Hedberg, Y. S.; Chromium and leather: a review on the chemistry of relevance for allergic contact dermatitis to chromium. *J. Leather Sci. Eng.* **2**, 20, 2020.
4. Ding, W., Yi, Y. D., Wang, Y. N., Zhou, J. F., Shi, B.; Preparation of a highly effective organic tanning agent with wide molecular weight distribution from bio-renewable sodium alginate. *ChemistrySelect* **3**, 12330-12335, 2018.
5. Wu, X. H., Qiang, X.H., Liu, D., Yu, L. D., Wang, X. K.; An eco-friendly tanning process to wet-white leather based on amino acids. *J. Clean. Prod.* **270**, 122339, 2020.
6. Shi, J. B., Zhang, R. Z., Mi, Z. Y., Lyu, S. Q., Ma, J. Z.; Engineering a sustainable chrome-free leather processing based on novel lightfast wet-white tanning system towards eco-leather manufacture. *J. Clean. Prod.* **282**, 124504, 2021.
7. Yu, Y., Wang, Y. N., Ding, W., Zhou, J. F., Shi, B.; Preparation of highly-oxidized starch using hydrogen peroxide and its application as a novel ligand for zirconium tanning of leather. *Carbohyd. Polym.* **174**, 823-829, 2017.
8. Gao, D. G., Cheng, Y. M., Wang, P. P., Li, F., Wu, Y. K., Lyu, B., Ma, J. Z., Qin, J. B.; An eco-friendly approach for leather manufacture based on P(POSS-MAA)-aluminum tanning agent combination tannage. *J. Clean Prod.* **257**, 120546, 2020.
9. Huang, W. L., Song, Y., Yu, Y., Wang, Y. N., Shi, B.; Interaction between retanning agents and wet white tanned by a novel bimetal complex tanning agent. *J. Leather Sci. Eng.* **2**, 8, 2020.
10. Chen, W. Y., Li, G. Y.; Tanning chemistry. Beijing: China Light Industry Press Ltd.; 2018.
11. Covington, A. D.; Tanning chemistry: the science of leather. Cambridge: Royal Society of Chemistry; 2011.
12. Yu, Y., Wang, Y. N., Ding, W., Zhou, J. F., Shi, B.; Preparation of highly-oxidized starch using hydrogen peroxide and its application as a novel ligand for zirconium tanning of leather. *Carbohyd. Polym.* **174**, 823-829, 2017.
13. Guo, X. R., Yu, Y., Wang, Y. N., Shi, B.; Oxidized maltodextrin: A novel ligand for aluminium–zirconium complex tanning. *JALCA*, **116**, 155-161, 2021.
14. Ramasami, T., Sreeram, J., Rao, J., Nair, B. U.; Approaches towards elucidating the mechanism of tanning using an organo-zirconium complex. *JALCA*, **95**, 359-367, 2000.
15. Cai, S. W., Zeng, Y. H., Zhang, W. H., Wang, Y. N., Shi, B.; Inverse chrome tanning technology based on wet white tanned by Al-Zr complex tanning agent. *JALCA*, **110**, 114-121, 2015.
16. Yu, Y., Wang, Y. N., Ding, W., Zhou, J. F., Shi, B.; Effect of catalyst on structure of hydrogen peroxide oxidized starch and its performance as a ligand in zirconium tanning of leather. *Fine Chemicals*, **35**, 1928-1934, 2018.
17. Yu, Y., Zeng, Y. H., Wang, Y. N., Liang, T., Zhou, J. F., Shi, B.; Inverse chrome tanning technology: a practical approach to minimizing Cr(III) discharge. *JALCA*, **115**, 176-183, 2020.
18. Tang, Y. L., Zhou, J. F., Zhang, W. H., Shi, B.; Existing forms of chromium in wastewater from leather finishing and its influence on elimination. *China leather*, **46**, 7-12, 2017.
19. Wang, Y. N., Huang, W. L., Zhang, H. S., Tian, L., Zhou, J. F., Shi, B.; Surface charge and isoelectric point of leather: A novel determination method and its application in leather making. *JALCA*, **112**, 224-231, 2017.
20. Song, Y., Wang, Y. N., Zeng, Y. H., Wu, H. P., Shi, B.; Quantitative determinations of isoelectric point of retanned leather and distribution of retanning agent. *JALCA*, **113**, 232-238, 2018.
21. Lei, C., Lin, Y. R., Zeng, Y. H., Wang, Y. N., Yuan, Y., Shi, B.; A cleaner deliming technology with glycine for ammonia-nitrogen reduction in leather manufacture. *J. Clean. Prod.* **245**, 118900, 2020.

Polyurethane Electrospun Fiber Biomimetics Membrane for Constructing the Structure of Grain Layer with Good Breathability for Cattle Split Leather

by

Nan Chen,[1,2] Yanchun Li,[1,2*] Jianbo Qu,[1,2*] Jian-Yong Wang[1,2]
[1]*School of Light Industry and Engineering, Qilu University of Technology (Shandong Academy of Science);*
[2]*Key Laboratory for Green Technology of Leather Manufacture,* China National Light Industry Council
No. 3501 Daxue Rd, Changqing District, 250353, Jinan, Shandong Province, China

Abstract

The traditional thick coating on split leather does not have the ability to breathe like full grain leather. The air and water vapor permeabilities of full grain leather are well known properties due to its fiber woven structure. Simulating the fiber morphology and weaving structure of the dermis or grain layer is very important to construct a top surface layer for split leather. In this paper, a PU (polyurethane) foam layer is put first on the split to enhance the adhesion of a second application of a superfine fibrous PU resin. This foam uses well-known waterborne polyurethane foaming technology. This dried foam has good breathability because of high porosity. A superfine fiber membrane is next put atop of the foam layer by using an electro-spun polyurethane resin. This second resin imitates collagen fibers in the network structure of the leathers' grain layer. Thus, this resultant electrospun fiber biomimetics membrane simulated the grain layer of natural leather. SEM showed the morphology and structure of this electrospun fiber biomimetic membrane to be like that of the grain layer of natural leather. The porosity and apparent density were basically the same as the grain of leather, which were 63.65% and 583.878 kg/m^3 respectively. The air and water vapor permeability of the biomimetics membrane were also as high as 2250 mL·cm^{-2}·h^{-1} and 8753.02 μg·cm^{-2}·h^{-1} respectively. Therefore, the biomimetics membrane largely restored the ability to breathe of split leather. Thus, this method simulates the performance and structure of full grain leather and is a novel method for industrial production.

Introduction

There is no comparison between the flat non-porous coating or finish on split leather with the natural grain layer of leather which has good breathability due to its disorderly and tightly woven fiber network structure. [1-3] In the tanning production process, the cattle leather is usually divided into the valuable top grain leather and the less-valued split leather through the splitting operation.[4] This resultant split leather has a low worth which needs to be recovered. Polyurethane (PU) resin is usually used to coat or finish the surface of split cattle leather.[5] The thick coating or finish on split leather, hides the morphology of the collagen fibers and closes its natural pores. Clearly, the finish seriously affects its ability to breathe and adversely impacts the handle [feels like plastic] of the finished leather.[6, 7] Therefore, the deposition on split of a biomimetics grain layer gives a fiber network woven structure which endows good breathability and can readily replace the traditional PU coating to enable a very broad application prospect.

Electrospinning technology continuously produces nano-scale fibers which were reported by many groups.[8-11] The electrospun fiber membranes prepared by electrospinning technology with good performance are widely used in textiles, packaging, filtration and other fields.[12,13] Electrospinning technology gives a disorderly-arranged and reticular braiding structure fiber membranes with similar structure, high porosity, good air and water vapor permeability compared with natural leather grain surface layer.[14-16] This also provides a guarantee for simulating the grain surface layer of natural leather and the resultant artificial grain surface or [biomimetics finish] imitating natural leather.

In this paper, the PU foam coating was prepared by using water-borne polyurethane foam technology. The topside of the split was thinly coated with this foam resin to get a high porosity structure [after drying] in order to ensure the ability to breathe, and to enhance the adhesion of electrospun fiber to it. The electrospinning technology used another polyurethane resin to deposit its biomimetics electrospun fibers on the foam first or basecoat. The selected biomimetics fibers have a similar structure to collagen fiber and are composed of a special network morphology like the grain layer of the leather. Thus, the electrospun fiber biomimetics-membrane is a topcoat which imitates the grain layer of the leather. The morphology and structure of the electrospun fiber biomimetic membrane was analyzed by SEM. It was similar to the grain layer of leather. The porosity and apparent density of the split coated with a foam basecoat and electrospun fiber biomimetics membrane topcoat were basically the same as the parent split leather. The air and water vapor permeability of the split coated with the biomimetics membrane are also nearly as high as the not coated split leather. By comparing

*Corresponding authors emails: qlulyc@126.com ; qujianbo396@sohu.com
Manuscript received January 28, 2021, accepted for publication March 21, 2021.

the fiber denier, horizontal weaving angle and morphology of the biomimetic membrane, the split leather coated with the biomimetics membrane has good air permeability and water vapor permeability. The biomimetics finish has a structure and a performance similar to the dermis grain surface layer. This novel biomimetics finish on split leather gave good breathability and has broad application prospects.

Experimental

Materials and Instruments

Polyurethane (6008D) was purchased from Xuchuan Chemical (Suzhou) Co., Ltd. Waterborne polyurethanes (2040 and 3485) were purchased from Wanhua Chemical Group Co., Ltd.

Electrostatic spinning machine (ET-2535H) purchased from Beijing Ucalery Co., Ltd. China. Desktop scanning electron microscope (Pure) made by Phenom Co.,Ltd., Netherlands and Hot field-emission scanning electron microscope (G500) made by Zeiss Co., Ltd. Germany. Fully automatic mercury porosimeter (PoreMaster-60GT) made by Quantachrome Co., Ltd. America. Screw micrometer (0-25mm 0.001mm) was purchased from Schut Co., Ltd. China. Leather air permeability tester (GT-7007-0) and Low-temperature penetration tester (GT-7045-EV) made by High-speed Railway Testing Instrument Co., Ltd. China.

Preparation of the biomimetics electrospun fiber coating

There are many fluff and fiber protrusions on the surface of the spilt cattle leather, which affect the adhesion of the material and need to be treated. The foaming liquid was prepared by waterborne PU (2040, 3458) through polyurethane foaming technology.[17-19] The foaming liquid was evenly and thin coated on the surface of split cattle leather after high-temperature ironing treatment, and dried and pressed flat at 60°C as the receiver of electrostatic spinning electrospun fiber.[20-22]

Using polyurethane resin (6008D) as the spinning dope, spinning for 3-4 hours was done under the condition of ventilation, positive electric high voltage of 25kV, negative electric high voltage of 5kV, liquid output speed 0.06mm/min, ambient temperature 30°C, humidity 40%. By adjusting the electrospinning angle, the electrospun fiber were evenly covered on the split cattle leather with foam coating, the preparation of PU electrospun fiber biomimetics membrane split cattle leather was finished. The preparation diagram is as follows:

Characterization

Morphology observation

The surface and longitudinal section morphology of full grain cattle crust leather (FGL), split cattle leather with traditional PU coating (PUSL) and PU electrospun fiber biomimetics membrane split cattle leather (NBSL) were analyzed by desktop scanning electron microscope and a hot field-emission scanning electron microscope.[23]

Porosity and apparent density analyses

The porosity of FGL, PUSL, NBSL were measured by fully automatic mercury porosimeter.[24] The apparent density of the fibers of FGL, PU foam coating split cattle leather (PUFSL), NBSL were measured by a screw micrometer through the size method.[25, 26]

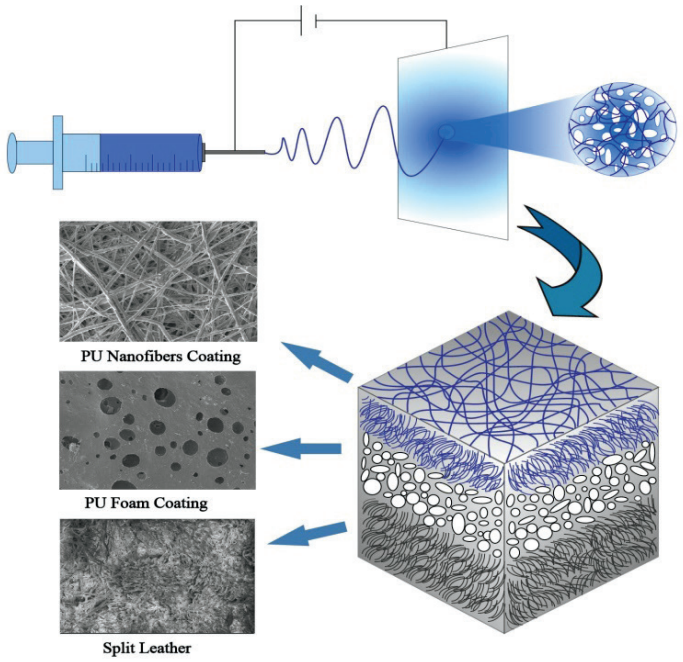

Figure 1. Schematic diagram of preparation of PU electrospun fiber biomimetics membrane split leather

The calculation formula of the size method is as follows:

$$\rho = \frac{m \cdot 10^6}{L \cdot W \cdot H} \quad (1)$$

Where: ρ — Apparent density, (Kg/m^3)

m — Sample quality (g)

L — Sample length (mm)

W — Sample width (mm)

H — Sample height (mm)

Air permeability and water vapor permeability analyses

The air permeability and water vapor permeability of split cattle leather (SL), PUSL, PUFSL, NBSL were tested by the leather air permeability tester and low-temperature penetration tester.[27] The air permeability and water vapor permeability of different materials were calculated by the following formula:

Air permeability calculation formula:

$$K = \frac{100 \times 3600}{10(t - t_0)} = \frac{36000}{t - t_0} \quad (2)$$

Where: K — Sample air permeability (ml/(cm^2•h))

t — The time required for the specified area of the sample to penetrate 100mL of air (s)

t_0 — Time required for blank experiment (s)

10 — Sample area through air (cm^2)

Water vapor permeability calculation formula:

$$P = \frac{7639 \times m}{d^2 \times t} \quad (3)$$

Where: P — Water vapor permeability (mg/(cm^2•h))

m — Increased mass of the test bottle twice (mg)

d — Inner diameter of test bottle (mm)

t — Time between two sample weighing (min)

Results and discussion

SEM observation of the surface and longitudinal of the sample

Figure 2a, 2b and 2c respectively are the surface morphology of FGL, PUSL, NBSL. We can see from the SEM pictures, the grain layer of FGL is horizontally woven by many fibers of different deniers (Figure 2a). The fiber diameter was about 300~800nm, inter-fiber porosity is obvious. The porosity was 65.55% tested by mercury porosimeter. This high pore fiber structure provides a good breathability of the leather.[28,29]

PU coating method is widely used in the production of split leather.[30,31] We can see from Figure 2b, the PU coating completely covered the surface of the split cattle leather, the coating has a flat, non-porous structure and lacks open pores communicating with the outside, which was quite different from the three-dimensional network structure of the grain layer fiber of leather. The closed structure greatly affects the ability of the split leather to breathe.

In order to solve the problem of poor breathability performance of the thick PU coating on the split leather,[32,33] PU electrospun fibers were prepared by electrospinning technology, and the derma grain layer was simulated from aspects of the size, structure and weaving mode (Figure 2c). The PU electrospun fiber diameter was 400~900nm, and the NBSL porosity was 63.65%, which all are very close to the fiber fineness and porosity of dermis grain layer. The PU electrospun fiber membrane was composed of two kinds of different denier fibers. The fibers with larger denier imitate the supporting effect of the thicker collagen fibers in the grain layer of leather, while the fibers with smaller denier imitate the network structure formed by the finer fibers in the grain layer of leather. Compared with the traditional PU coating, the electrospun fiber membrane was closer to the natural leather grain layer in morphology, while ensuring the fiber weaving, it retains more pores and has a weaving angle similar to that of dermis grain layer fibers.[34] In addition, by calculating the apparent density of the biomimetics electrospun fiber membrane, it is found that the biomimetics membrane has a fiber weave density similar to that of leather (Figure 3), which achieves a high degree of simulation in structure.

PU electrospun fiber membrane was prepared by electrospinning technology to simulate the reticular braiding structure of pellet surface fiber. Its fibers are very close to collagen fibers in fiber morphology, size, fiber weaving angle and density. The disordered fibers produced by electrospinning technology due to the interaction of charges also provide sufficient pores for the biomimetic PU electrospun fiber membrane.[35,36] From the structure point of view, the PU electrospun fiber-biomimetics membrane can greatly retain the ability to breathe of the split leather.

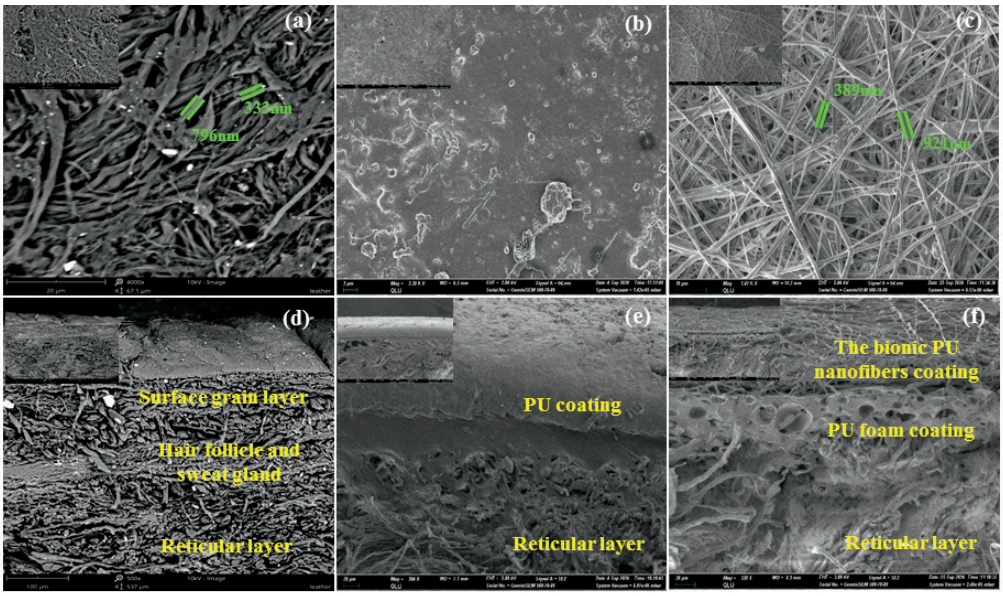

Figure 2. **(a)** SEM of the surface of FGL. **(b)** SEM of the surface of PUSL. **(c)** SEM of the surface of NBSL. **(d)** SEM of longitudinal section of FGL. **(e)** SEM of longitudinal section of PUSL. **(f)** SEM of longitudinal section of t NBSL.

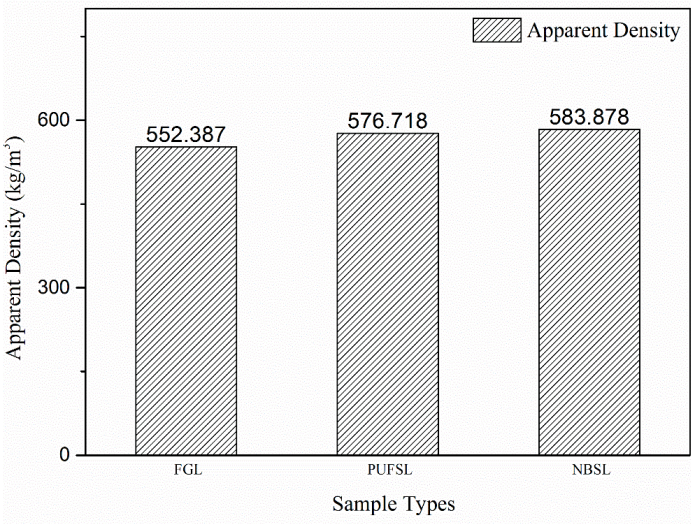

Figure 3. The apparent density was compared by the size method.

The longitudinal sections of FGL, PUSL, NBSL were analyzed by SEM (Figure 2d, e, f), we can see the changes in the fiber structure of three different types of leather more intuitively.

From Figure 2d, we can clearly see the fiber network structure in the grain layer in the longitudinal section of the leather, the fibers are arranged tightly and disorderly, and the pores left after removing the hair follicles and sweat gland tissues by the tanning process can be seen. The coating of PUSL was a flat non-porous PU film with no fiber cross-section structure, which was an indivisible whole (Figure 2e). The coating of NBSL has a clear fiber section and obvious inter-fiber pores, which was very similar to the natural leather grain surface fiber in morphology (Figure 2f). The thin PU foaming layer on the surface of the split leather coated by water-based polyurethane foaming technology form a porous structure. This porous structure is similar in appearance to the cavity left by removing the hair follicles and sweat gland during tanning and also the adhesion of the subsequent electrospun fiber biomimetic membrane to the foaming is improved. From the structural point of view, the breathing ability of leather can be retained.

Test for Air permeability and water vapor permeability

The good air permeability and water vapor permeability of leather are currently difficult to achieve by other materials.[37] While preparing the artificial grain layer for the split leather, the good air and water vapor permeability of the leather should be retained as much as possible. In this research, the air permeability and water vapor permeability of various coatings are compared by experiments and calculations. The results are shown in Figure 4.

It can be clearly seen from Figure 4 that the PU coating (PUSL) greatly decreases the original air permeability and water vapor permeability of the split leather (SL). The water-based PU foaming coating (PUFSL) has little effect on the air permeability and water vapor permeability of the split leather. The NBSL which has a high degree of simulation with the grain layer of leather in structure, has good air permeability and water vapor permeability, it guarantees the ability of the split cattle leather to breathe.

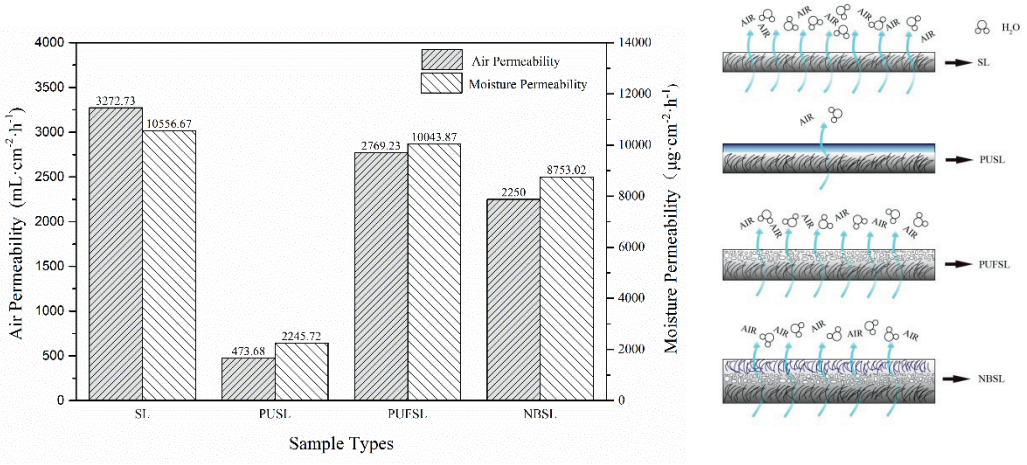

Figure 4. Comparison of air permeability and water vapor permeability of SL, PUSL PUFSL and NBSL.

Conclusions

In summary, a practical method to simulate the structure of the dermal grain layer was proposed. By way of using electrospinning technology, a PU electrospun fiber biomimetics membrane was coated on split cattle leather. It simulated the grain layer of the leather by constructing a three-dimensional woven structure like that of the dermis. Split cattle leather coated by this PU electrospun fiber biomimetics finish has good air and water vapor permeability compared with the traditional thick PU coat on split leather. This novel biomimetic finishing approach is useful to produce split leather of high value, and with the ability to breathe and thus has broad application prospects. There is still a lot of work to be done in the future. We will further research various physical and mechanical properties of the coating, including its adhesion by improving the electrospinning method and other influence factors in order to increase its application properties.

Acknowledgements

Shandong Provincial Key R&D Program/Major Science and Technology Innovation Project of Shandong Province (2019JZZY020230)

References

1. S, Montelli., L, Corain., B, Cozzi., and A, Peruffo., Histological analysis of the skin dermal components in bovine hides stored under different conditions, *JALCA* **110,** 54-60, 2015.
2. Li, X. X., Wang, Y. N., Li, J. and Shi, B., Effect of sodium chloride on structure of collagen fiber network in pickling and tanning, *JALCA* **111,** 230-237, 2016.
3. Li, Z., Denis, P. and Yang, J. S., Mechanical behaviour of natural cow leather in tension, *AMSS*, **22,** 37-44, 2009.
4. Xu, W. X., Zeng, H., Zhou, J. F., Wang, Y. and Shi, B., The reinforcement of leather split by constructing an interpenetrating network via in-situ recombination of PVA, *JALCA* **113,** 255-263, 2018.
5. Liu, C. K., L. N., Preparations of nonwoven and green composites from collagen fibrous networks, *JALCA* **109,** 35-40, 2014.
6. Wu, Y., Wang, A. H., Zheng, R. R., Tang, H. Q., Qi, X. Y. and Ye, B., Laser-drilled micro-hole arrays on polyurethane synthetic leather for improvement of water vapor permeability, *Appl. Surf. Sci.*, **305,**1-8, 2014.
7. Chen, Y., Fan, H., Liu, R. and Yuan, J., Nano-SiO_2 in-situ hybrid polyurethane leather coating with enhanced breathability, *Fibers Polym,* **11,** 241-248, 2010.
8. Yuan, H., Zhao, S., Tu, H., Li, B., Li, Q., Feng, B. and Peng, H., et al., Stable jet electrospinning for easy fabrication of aligned ultrafine fibers, *J. Mater. Chem,* **22,** 19634, 2012.
9. Mirjalili, M. and Zohoori, S., Review for application of electrospinning and electrospun nanofibers technology in textile industry, *J. Nanostruct. Chem,* **6,** 207-213, 2016.
10. Barzegar, F., Bello, A., Fabiane, M., Khamlich, S., Momodu, D., Taghizadeh, F. and Dangbegnon, J., et al., Preparation and characterization of poly(vinyl alcohol)/graphene nanofibers synthesized by electrospinning, *J. Phys. Chem. Solids,* **77,** 139-145, 2015.

11. Wang, C., Wang, J., Zeng, L., Qiao, Z., Liu, X., Liu, H. and Zhang, J., et al., Fabrication of electrospun polymer nanofibers with diverse morphologies, *Molecules,* **24,** 834, 2019.
12. Yu, X., Li, Y., Wang, X., Si, Y., Yu, J. and Ding, B., Thermoconductive, moisture-permeable, and superhydrophobic nanofibrous membranes with interpenetrated boron nitride network for personal cooling fabrics, *ACS Appl. Mater. Interfaces,* **12,** 32078-32089, 2020.
13. Sáenz-Pérez, M., Bashir, T., Laza, J. M., García-Barrasa, J., Vilas, J. L., Skrifvars, M. and León, L. M., Novel shape-memory polyurethane fibers for textile applications, *Text. Res. J.* **89,** 1027-1037, 2019.
14. Guan, Q., Ling, Z., Han, Z., Yang, H. and Yu, S., Ultra-strong, ultra-tough, transparent, and sustainable nanocomposite films for plastic substitute, *Matter,* **3,** 1308-1317, 2020.
15. Jiang, G., Luo, L., Tan, L., Wang, J., Zhang, S., Zhang, F. and Jin, J., Microsphere-fiber interpenetrated superhydrophobic PVDF microporous, *ACS Appl. Mater. Interfaces*, **10,** 28210-28218, 2018.
16. Wang, J., Li, Y., Tian, H., Sheng, J., Yu, J. and Ding, B., Waterproof and breathable membranes of waterborne fluorinated polyurethane modified electrospun polyacrylonitrile fibers, *RSC Adv.,* **4,** 61068-61076, 2014.
17. Zhao, B., Qian, Y., Qian, X., Fan, J. and Feng, Y., Fabrication and characterization of waterborne polyurethane/silver nanocomposite foams, *Polym. Compos.,* **40,** 1492-1498, 2018.
18. Liu, X., Wang, J., Huang, K. and Li, F., Experimental study on dynamic water grouting of modified water-soluble polyurethane, *Can. J. Civ. Eng.,* **23,** 3897-3906, 2019.
19. Kaushiva, B. D., McCartney, S. R., Rossmy, G. R. and Wilkes, G. L., Surfactant level influences on structure and properties of flexible slabstock polyurethane foams, *Polymer,* **41,** 285-310,2000.
20. Engels, H., Pirkl, H., Albers, R., Albach, R. W., Krause, J., Hoffmann, A. and Casselmann, H., et al., Polyurethanes: Versatile Materials and Sustainable Problem Solvers for Today's Challenges, *Angew. Chem., Int. Ed*., **52,** 9422-9441, 2013.
21. Chandan, M. R., Radhakrishnan, K., Bal, D. K., Rizwan, M. and Shaik, A. H., Flexible polyurethane foam-ZnO nanocomposite for photocatalytic degradation of textile dye, *Fibers Polym.,* **21,** 2314-2320, 2020.
22. Dixit, S., Yadav, A., Dwivedi, P. D. and Das, M., Toxic hazards of leather industry and technologies to combat threat: a review, *J. Cleaner Prod.,* **87,** 39-49, 2015.
23. Bittrich, E., Schladitz, K., Meyndt, R., Schulz, H. and Godehardt, M., Micro-computed tomography studies for three-dimensional leather structure analysis , *JALCA* **109,** 367-371,2014.
24. Li, X. X., Wang. Y.N., Li, J. and Shi, B., Effect of sodium chloride on structure of collagen fiber network in pickling and tanning, *JALCA* **111,** 230-237, 2016.
25. Minju, N., Jobin, G., Savithri, S. and Ananthakumar, S., Double-silicate derived hybrid foams for high-capacity adsorption of textile dye effluent: statistical optimization and adsorption studies, *Langmuir,* **35,** 9382-9395, 2019.
26. Le Gall, M., Davies, P., Martin, N. and Baley, C., Recommended flax fibre density values for composite property predictions, *Ind. Crops Prod.,* **114,** 52-58, 2018.
27. Keyong,T., Fang, W., Jie, L. and Weihua, F., Study on the air permeability of leather [J], *China Leather,* **31,** 17-19, 2002.
28. Sathish, M., Bubansewari, T. S., Rao, J. R. and Fathima, N. N., Effect of syntan to fatliquor ratio on porosity and mechanical properties of wet-blue leather, *JALCA* **112,** 121-127, 2017.
29. Kelly, S. J., Edmonds, R., Cooper, S., Sizeland, K. H. and Wells, H. C., Mapping tear strength and collagen fibril orientation in bovine, ovine and cervine hides and skins, *JALCA* **113,** 1-11, 2018.
30. Tian, S., Recent advances in functional polyurethane and its application in leather manufacture, *A Review, Polymers,* **12,**1996, 2020.
31. Zheng, G. K., Lu, M., Rui, X. P. and Sun, Y. X., The effect of acrylate on structure and properties of waterborne polyurethane porous coated fabrics, *J. Appl. Polym. Sci.,* **135,** 45783, 1-11, 2018.
32. Shi, H. H., Chen, Y., Fan, H. J., Xiang, J. and Shi, B., Thermosensitive polyurethane film and finished leather with controllable water vapor permeability, *J. Appl. Polym. Sci.,* **117,** 1820-1827, 2010.
33. Li, X., Zhang, Y., Feng, H., Guo, J. and Li, H., Research current situation and development of polyurethane coatings, *Applied Chemical Industry,* **39,** 1091-1095, 2010.
34. Zhang, H. Y. and Li, T. D., 3D Reconstruction method of leather fiber bund weaving network, *JALCA* **113,** 248-254, 2018.
35. Yu, D. G., Wang, M., Li, X., Liu, X., Zhu, L. M. and Annie Bligh, S. W., Multifluid electrospinning for the generation of complex nanostructures, *Nanomed. Nanobiotechnol.,* **12,** 1-11, 2020.
36. Xue, J., Wu, T., Dai, Y. and Xia, Y., Electrospinning and electrospun nanofibers: methods, materials, and applications, *Chem. Soc. Rev.,* **119,** 5298-5415, 2019.
37. Nam, C. and Lee, Y., Multilayered cellulosic material as a leather alternative in the footwear industry, *Text. Res. J.,* **37,** 20-34, 2018.

Development of a Headspace-Solid Phase Micro Extraction Method for the Analysis of Volatile and Semi-Volatile Organic Compounds from Polyurethane Resins for Leather Finishing

by

Antonia Flores, Sílvia Sorolla, Concepció Casas, Rosa Cuadros and Anna Bacardit

A³ Leather Innovation Center. Escola Politècnica Superior. Departament d'Informàtica i Enginyeria Industrial. Universitat de Lleida. Avda. Pla de la Massa, 8. 08700-Igualada

Abstract

Volatile organic compounds (VOCs) and Semi-Volatile Organic Compounds (SVOCs) arise from the chemicals used in the various stages of the leather manufacturing process. An important aim of the tanning industry is to minimize or eliminate VOCs and SVOCs, without lowering the quality of leather.

This paper shows the development of a new headspace-solid phase micro extraction coupled with gas chromatography–mass spectrometry (HS-SPME/GC-MS) method for the identification of VOCs and SVOCs emitted by newly designed polymers for the leather finishing operation. These new polymers are polyurethane resins designed to reduce the VOC and SVOC concentration. This method enables a simple and fast determination of the qualitative and semi-quantitative content of VOCs and SVOCs in polyurethane-type finishing resins. The chemicals that are of concern in this paper are the following: Dipropylene glycol Monomethyl Ether (DPGME), DBE-3 (a mixture of dibasic esters) and Triethylamine (TEA). The test conditions that have been determined to carry out the HS-SPME assay are the following: incubation time (2 hours), extraction temperature and time (40°C; 5 minutes) and the desorption conditions (280°C, 50 seconds).

Ten samples of laboratory scale resins were tested by HS-SPME followed by gas chromatography (GC-MS). DPGME and DBE-3 (a mixture of dimethyl adipate, dimethyl glutarate and dimethyl succinate) have been identified effectively. The compounds are identified by a quantitative method using external calibration curves for the target compounds. The technique is not effective to determine the TEA compound, since the chromatograms shown poor resolution peaks for the standard.

Introduction

Volatile Organic Compounds (VOCs) are hydrocarbons present in gaseous state at room temperature, or which are highly volatile at this temperature. VOCs refers to any compound of carbon, excluding carbon monoxide, carbon dioxide, carbonic acid, metallic carbides or carbonates, and ammonium carbonate, which participates in atmospheric photochemical reactions. VOCs play an important role in the environment and human health.[1] The health consequences can vary greatly, since it depends on the nature of the chemical compound, the degree of danger and the period of exposure to it; these consequences can range from the absence of known effects to a degree of severe toxicity.[2] The main concern with this type of compound is that some of them may become carcinogenic, mutagenic and reprotoxic (CMR) substances. In addition, some VOCs may cause annoying odors that, depending on the olfactory capacity of each human being, can cause rejection or mistrust among consumers. The environmental effects caused by VOC emissions are a matter of concern at the atmospheric level, since they destroy the ozone layer and, together with nitrogen oxides and sunlight, are precursors of tropospheric ozone formation and also produce the well-known photochemical smog.[1,3]

With the aim of reducing the adverse effects caused by VOC emissions, the European and Spanish legislation through the Directive 2010/75/EU and the Royal Decree 117/2003 regulates, limits and details a series of provisions for facilities and activities where organic solvents are used in their production processes.[1]

VOCs and SCOVs emissions are controlled by the legislation through the Annex VII of Directive 2010/75/EU, Activity No 13; being the limit from 75 to 150 g of solvent emitted per m^2 of leather product produced. The VOC emission levels to be in conformity with the Best Available Techniques (BAT) for the leather production in Europe are between 10-25 g/m^2 expressed as annual average values.

Organic solvents are used in certain stages of leather manufacturing, such as in post-tanning and especially during the finishing operations. Due to the current legislation, environmental problems, possible health effects and irritating odors that VOC emissions can generate, this sector is implementing improvements in the production system, minimizing or substituting solvent-based chemicals for less harmful products, to obtain a sustainable leather product, and preserving the highest quality. Even with these measures, leather finishing products are applied in concentrated quantities, which implies that VOC emissions can occur. For this reason, it is important to

Corresponding author email: anna.bacardit@udl.cat
Manuscript received February 1, 2021, accepted for publication March 28, 2021.

develop an analytical method to identify the presence of VOCs and Semi-Volatile Organic Compounds (SVOCs) compounds in finishing chemicals to go forward with the identification of critical compounds and to ensure that new polyurethane resins will comply with the expectations.[4]

One of the most widely used techniques for the determination of VOCs and SVOCs is Gas Chromatography coupled to Mass Spectrometry (GC-MS). The combination of high resolution, sensitivity and relatively short analysis time make the technology a routine used in most chemical laboratories.[5,6] Before the chromatographic analysis, the chemical compounds must be isolated and/or extracted from the matrices to be tested, being different techniques for this purpose; such as Liquid-Liquid extraction, Purge and Trap (P&T) or Solid Phase Extraction (SPE). Although some of these methods are useful for VOCs and SVOCs analysis, they have certain drawbacks, such as the sample handling and sample preparation time. Solvents are used in some of these extraction procedures and therefore, it must be managed correctly after the analysis. For this reason, VOC analytical testing techniques have improved and evolved to develop methods in which sample handling is minimal and practically zero solvent consumption.[7,8]

Pawliszyn and his colleagues developed the methodology in the early 1990s as a new method of sampling and sample preparation for further analysis by chromatography, which was later expanded by Zhang and Pawliszyn with the Headspace extraction modality (HS).[9-12] The HS sampling modality is applicable to both solid and liquid samples when the objective is the determination of volatile organic compounds in the sample or when the matrix is complex, since in this modality of extraction the fibber exposure to the sample is made without contact with the sample, thus extending its useful life.[13-15] Since its inception, this technique has been applied in various areas such as the environment, food, aromas and perfumes and also in pharmaceuticals. Among these, approximately 40% focus on applications about the environment and the amount of literature on this topic increases every year.[9]

Experimental

Chemicals and reagents

To assist the leather industry to improve production processes, a water-based synthesis of eleven polyurethane resins for the finishing of leather was developed in a pilot scale reactor. The substitution of organic solvents of great environmental concern by less harmful chemicals is one of the focus of this research. As the newly designed resins have to be analysed to determine their VOCs and SVOCs content, the start-up and performance of a test method to determine those compounds is of a great importance. The resins are identified from NV001 to NV011. NV001 resin is used as a reference for the HS-SPME method optimization.

This study is focused on three chemical compounds used in the synthesis of resins, which are the following: Dipropylene Glycol Monomethyl Ether (DPGME), DBE-3 (mixture of the dibasic esters dimethyl adipate, dimethyl glutarate and dimethyl succinate) and Triethylamine (TEA). It is emphasized that these chemical compounds are not routinely tested in laboratories. For this reason, this research is focussed to develop, optimize and validate a specific method of analysis by using the HS-SPME/GC-MS techniques.

Dipropylene Glycol Monomethyl Ether (DPGME) with a boiling temperature of 190°C and CAS No. 34590-94-8 is a mixture of isomers. The composition of the substance is as follows: 40-50% 1-(2-methoxypropoxy) -2-propanol (CAS No. 13429-07-7), 40-45% 1- (2-methoxy-1-methylethoxy) -2-propanol (CAS No. 20324-32-7), 2-5% 2- (2-methoxypropoxy) - 1-propanol (CAS No. 13588-28-8) and 3-5% 2- (2-methoxy-1-methylethoxy) -1-propanol (CAS No. 55956-21-3). These isomers are not purchased separately, which implies that the standard used in the study is Dipropylene glycol methyl ether, mixture of isomers (97%) (Sigma-Aldrich).

DPGME has low oral toxicity, both dermal and inhalation, and has no carcinogenic, reprotoxic, or mutagenic effects in humans. At the environmental level it is considered an easily biodegradable product in aerobic conditions, but only slightly degradable in anaerobic conditions. This chemical compound is often used in the manufacture of paints, varnishes, inks, and cleaners.[16]

The commercial product DBE-3 with CAS No. 95481-62-2 is a mixture of dibasic esters with a boiling range of 215-225°C, the composition of which is as follows: 89% dimethyl adipate (CAS No. 627-93-0), 10% dimethyl glutarate (CAS No. 1119-40-0) and 1% dimethyl succinate (CAS No. 106-65-0). Commercial standards for each component are purchased separately with a purity of> 99% (Sigma-Aldrich). This solvent is easily biodegradable, environmentally friendly and of low toxicity. DBE-3 can be a good alternative to conventional VOC-emitting solvents, including isophorone, glycol ethers, and glycol ether acetate, ketones with high boiling point, dichloromethane, butyl diglycol, acetone and cyclohexanone. This solvent is usually used in the synthesis of paints, coatings, lubricants and strippers, among other uses.[14,15]

TEA is an aliphatic amine with a boiling point of 90°C, CAS No. 121-44-8. It was purchased as a standard with a purity of ≥ 99% (Sigma-Aldrich). Like other amines, it presents an ammoniacal odour. The vapors given off by this chemical are dangerous to health, and they can irritate the nose, throat and lungs; and therefore, its handling must be carried out carefully. This compound can cause allergies and skin rashes if prolonged exposure occurs, and causes irritation in case of eye contact, being advisable to wear suitable clothing during its handling.[17]

For the extraction of the analytes, a syringe with a fiber packing is used and the selectivity and sensitivity of the extraction method depend on the composition of this fiber. In this work Carboxene / Polydimethylsiloxane SPME Sampling Fiber (CAR-PDMS) 75 µm from Supelco was used. Additionally, 20 mL vials and silicone / PTFE septums of SPME for testing of samples (Thermo-Scientific) and a Magnetic stirrer, stirring and heating bloc (Selecta) were used.

Chromatography

Detection of VOCs and SCOVs was performed by using a Gas Chromatograph (GC) from Agilent Technologies (Agilent 7820A) equipped with a single quadrupole Mass Spectrometry (MS) detector (Agilent 5975MSD). The chromatographic column used is a DB-5MS column (122-5532 Agilent Technologies, 30m length×0.25µm film×0.250 mm diam.)

A manual injection of the SPME fiber was made into the injection port of the chromatograph (Agilent Technologies, 7820A GC system). The carrier gas was helium at a constant flow of 1.2 ml/min. The injector temperature was 280°C; the oven temperature program started at 55°C for 1 minute followed by two ramps. The first ramp was an increase of 6°C/min until reaching 180°C, followed by another increase of 15°C/min until reaching 230°C for 3 minutes. It works with a Split 1:200 and the data acquisition was done in SCAN mode with a m/z range of 30-300. The identification of the compounds was carried out by means of the NIST 14 mass spectral library (version 2.2) followed by the corresponding standards injection.

HS-SPME Method

A diluted sample with ultrapure water of the resin was placed and sealed into a 20ml vial with a Teflon septum. The diluted sample was stirred during a determinate period (incubation time) to achieve the equilibrium conditions. VOCs and SCOVs were transferred to the air phase into the sealed vial, known as Head Space (HS). When the incubation time was finished, the compounds were extracted from the vial using the CAR-PDMS fiber (75 µm) for a certain period (exposition time) and a determinate temperature (extraction temperature). Once this step was completed, the SPME fiber was placed into the GC injection port to desorb the VOCs and SVOC compounds adsorbed by the fiber. The desorption temperature and the desorption time were also established during the method development. After the desorption process, the fiber was conditioned until the next analysis (300°C, 5min.).[15]

Optimizing the HS-SPME/GC-MS test conditions

SPME fiber

After the extraction process, the SPME fiber contained VOC and SVOC compounds. The selectivity and sensitivity of the extraction method depends on its composition. Conventional fibers for SPME consist of a silica fiber wrapped with a sorbent material, such as PDMS (polydimethylosiloxane), PA (polyacrylate), DVB (divinylbenzene), CW (cabowax) and CAR (carboxen) among others. In the last 20 years, these fibers have been improved and commercialized.[11,19]

The solid phase micro extraction (SPME) is a sample preparation technique used for the extraction of VOCs and SVOCs for many applications, coupled with gas chromatography to elute and determine these types of compounds in solid and liquid samples. The main advantages of this technique are speed, high sensitivity; it does not require sample handling or solvent extraction procedures being environmentally friendly extraction technique, speeds up the separation, and increases throughput. In addition, this technique is extremely cost-efficient in comparison to alternate extraction methods.

Previous research from A^3 Leather Innovation Center regarding the applications of the SPME technique for the determination of VOC and SCOV compounds, suggest that the most suitable fiber type is the CAR/PDMS 75 µm.[4] Other previous research work also recommend this type of fiber for VOC extraction.[9,20] The terms of use of the SPME fiber given by the supplier (Sigma-Aldrich) also bring recommendations to choose the fiber depending on the compounds to be identified and quantified. Before the first use of the SPME sampling fiber, it must be conditioned at 300°C during 30 minutes into the GC injector.

Sample stirring

Sample stirring favors the mass transport between the sample and the fiber coating; providing shorter extraction times and greater sensitivity in pre-equilibrium extractions. There are different stirring methods, such as magnetic stirring or vortex stirring; each having advantages and disadvantages. Ultrasound technology is not recommended, as it can heat the sample uncontrollably and damage the sampling fiber. To obtain reproducible results, it is important to maintain the same agitation, method and intensity.[13]

The stirring is finally established at 500 rpm in a stirring and heating unit, which does not imply a large investment.

Sample preparation

The SPME test methodology does not require sample manipulation. During the test condition optimization, the sample provides a too large area in the eluted sample, thus forcing to aqueous dilute the resin samples in ultrapure water of Milli-Q quality to obtain the optimum chromatographic signal. When selecting the appropriate sample volume to introduce into the sealed SPME vial, it must be selected to leave sufficient free space on the top of the sealed vial (Head Space). Therefore, the sample volume must be sufficient to be representative, but not to exceed the headspace of the vial.[13] Sample volumes between 1 and 5 ml were studied. The optimum sample was established at 3 ml, leaving enough space at the top of the vial (Head Space), and providing the optimum chromatographic signal.

Table I

Relation between the incubation time and eluted area for DPGME isomers

Incubation time (min.)	Area DPGME Isomer 1/Tr. 6.5 min	Area DPGME Isomer 2/Tr. 6.9 min
30	65,553,724	60,229,962
60	238,710,132	221,139,978
120	**374,986,795**	**361,222,771**
180	67,968,336	63,434,754

Time exposure

After the equilibrium phase of VOCs and SCOVs between the liquid phase and HS, the SPME fiber was introduced into the space of the sealed vial without contact with the liquid sample. NV001 resin was used to start up the test conditions. As it is shown in table I, the incubation time was determined in 2 hours at room temperature, since the optimum response was observed for the compounds object of concern. The HS-SPME remained at room temperature because the presence of volatile substances towards the Headspace of the vial was observed by means of vapor generation at 23-25°C. Two major peaks are eluted in the chromatogram, which corresponds to the isomers of DPGME. Although these isomers are known from the literature,[22] it is not possible to differentiate one from the other by the GC-MS technique.

As can be seen in the results shown in Table I, the fiber is saturated and produces a logarithmic signal giving a maximum point which in this case is at 120 minutes. From this point on, the signal decreases. Therefore, to optimize the assay, the optimum point must be sought, and in this case the incubation conditions of the sample are set at 120 minutes.

Extraction conditions

The extraction time is one of the most critical parameters in the SPME technique. The determination of the optimal extraction time depends mainly on the objective of the analysis.

If the main objective is to obtain a high productive level of analysis, it is necessary to work in pre-equilibrium conditions, which implies a shorter extraction time. In this case, it is essential to keep the same extraction and stirring times for each sample. If the exposure time varies during sampling, it will imply poor reproducibility. Consequently, it is advisable to use an automated SPME system when working under pre-equilibrium conditions in order to achieve good reproducibility. On the other hand, if the objective of the test is to obtain good sensitivity and reproducibility, it must work under equilibrium conditions Once equilibrium is reached, the amount of the compounds absorbed by the fiber remains constant. This fact implies that extraction can be performed both automatically and manually.[13]

The objective of this experimentation is to develop and validate a method for the determination of VOC and SCOV by HS-SPME, which implies good reproducibility and sensitivity. For this reason, it is preferable to establish the incubation time and afterwards, start to study the extraction time. Three different extraction times were tested, 3, 5 and 10 minutes.

Previous research made by the A^3 Leather Innovation Center of VOC content in leather revealed that the extraction temperature also influences the test. In the analysis of the resins object of concern, temperatures of 40°, 65° and 80°C are investigated.[4]

The optimum extraction time was established in 5 minutes, being the optimum extraction temperature 40°C; as it is shown in Tables II and III. A chromatogram with two major peaks is obtained, which after the analysis of the DPGME standard it is confirmed to correspond to the Dipropylene Glycol Monomethyl Ether isomers.

In Table I the incubation conditions of the samples were set. From the results obtained in Table II, the extraction time conditions are

Table II

Extraction time and eluted area for DPGME isomers

Extraction time (min.)	Area DPGME Isomer 1/Tr. 6.5 min	Area DPGME Isomer 2/Tr. 6.9 min
3	15,916,774	15,636,472
5	**22,455,845**	**21,768,777**
10	20,253,580	20,042,077

Table III

Extraction temperature and eluted area for DPGME isomers

Extraction temperature (°C)	Area DPGME Isomer 1/Tr. 6.5 min	Area DPGME Isomer 2/Tr. 6.9 min
40	**83,582,114**	**73,845,294**
65	12,273,871	12,674,859
80	17,785,430	17,947,846

set. As can be seen in the results of Table II, the maximum signal obtained in area is at 5 minutes. As in incubation conditions, a logarithmic signal is produced with a maximum point, after which the signal loses intensity.

Table III shows the results to set the temperature conditions. As can be seen, the maximum signal obtained is at 40°C, also producing a logarithmic signal.

Therefore, the final conditions that were set to optimize the analysis were 120 minutes of incubation of the sample, 5 minutes of extraction of the sample at 40°C.

Desorption and fiber reconditioning

Once the compounds are absorbed into the SPME fiber, the next step is to desorb those compounds in the gas chromatograph for their elution and determination by GC-MS. Desorption step is made into the injection port of the GC, using a specific liner for SPME methodology. The variables influencing the desorption process are time and temperature. The desorption temperature varies according to the type of sampling fiber used, since it depends on the fiber coating material. According to the manufacturer, the recommended desorption temperature range for CAR / PDMS 75 µm fiber is from 250° to 310°C. In this experimentation, the tested desorption temperatures were the following: 250°, 265° and 280°C. According to the results of Table IV, 280°C was established as the optimal desorption temperature. Once the desorption process is finished, the fiber is kept in the injection port for 10 minutes for conditioning and/or automatic cleaning between samples, without the need to manually enter said temperature, thus saving time by unifying two processes in one.

The tested desorption times were 40, 50 and 60 seconds. Although the initial desorption time was 40 seconds, the resolution observed of both DPGME isomers improves with a desorption time of 50 seconds, as shown in Table V. According to the manufacturer's recommendations, desorption time improves with longer times, a fact also observed in previous studies from the A[3] Leather Innovation Center.[4]

Table IV

Desorption temperature and eluted area for DPGME isomers

Desorption temperature (min.)	Area DPGME Isomer 1/Tr. 6.5 min	Area DPGME Isomer 2/Tr. 6.9 min
250	**220,075,820**	**168,452,741**
265	213,603,258	165,858,258
280	192,478,282	152,641,200

Table V

Desorption time and eluted area for DPGME isomers

Desorption time (seg.)	Area DPGME Isomer 1/Tr. 6.5 min	Area DPGME Isomer 2/Tr. 6.9 min
40	**194,825,462**	144,200,024
50	192,478,282	**152,641,200**
60	189,284,028	142,425,646

Table VI

Optimised conditions for the HS-SPME assay of polyurethane resins

SPME fiber	Units	CAR/PDMS 75µm
Sample volume	ml	3
Incubation time	hour	2
Stirring speed	rpm	500
Extraction temperature	°C	40
Extraction time	min.	5
Desorption temperature	°C	280
Desorption time	seconds	50
Fiber conditioning at 280°C	min.	10

Results

HS-SPME/GC-MS optimized method for VOV and SVOC determination

Once all the variables that influence the determination of VOC and SCOV have been optimized using the HS-SPME extraction methodology, it is concluded that the established test parameters are those indicated in Table VI.

Analytical calibration and quantification

Once the HS-SPME method was established for the extraction of volatile compounds and subsequent identification by GC-MS, all the aqueous-based resins from NV002 to NV011 were tested in duplicate. The identification of the compounds object of concern was primarily made by comparing their mass spectrum with the NIST database of compounds. Next, a verification of the target compounds was made reproducing the test conditions with the standards. Figure 1 shows the chromatogram of the resin NV004.

In Table VII, the two DPGME isomers, dimethyl glutarate and dimethyl adipate were identified.

It was observed that dimethyl succinate did not appear in the chromatograms of the resin samples.

Its exhaustion during the resin synthesis and/or the lower concentration in the commercial products are probably the causes of this phenomenon. On the other hand, just two of the four isomers of the commercial DPGME standard were detected and quantified.

Although triethanolamine is present in all the synthesized resins, a very poor resolution of this compound was observed in the chromatographic results, affecting its quantification. Determination of low-molecular weight amines by gas chromatography implies additional risks due to their high aqueous solubility, volatility, polarity and basic character. As the molecular mass of amine

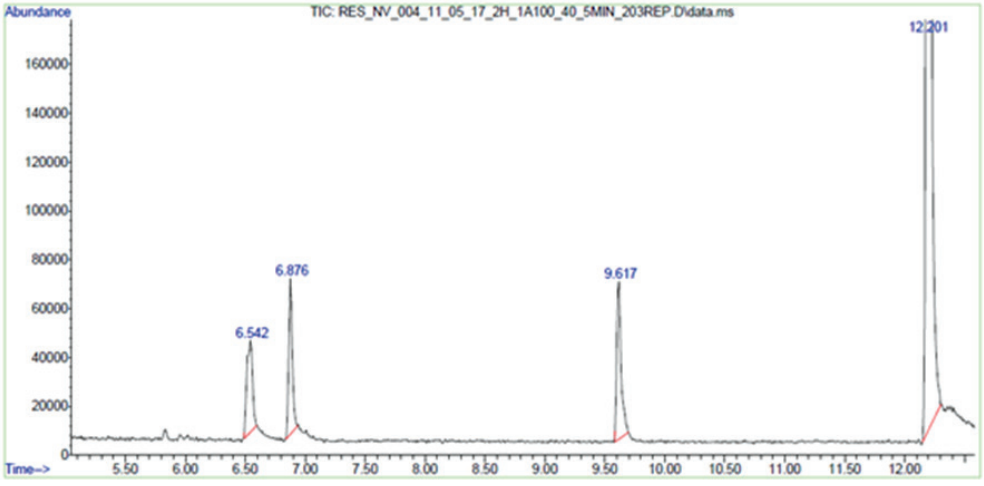

Figure 1. Resin NV004 chromatogram by HS-SPME/GC-MS

Table VII

Identification of VOC compounds from NV004 by HS-SPME/GC-MS

Peak	Ret. time (min.)	Area	% Area from total eluted	NIST identification	CAS Number
1	6.542	1,186,411	4.4	DPGME	Isomer 1
2	6.876	1,266,801	4.7	DPGME	Isomer 2
3	9.617	1,488,702	5.5	Dimethyl glutarate	1119-40-0
4	12.201	23,272,558	85.5	Dimethyl adipate	627-93-0

Table VIII

Calibration curves by external standard from the four target compounds

Compound	Concentration (mg/L)	R^2	Linear regression (Y= aX + b)
Dimethyl adipate	26.2 – 62.1 – 124.1 – 310.4 – 697.0 – 1241.4	0.9987	Y= 35265X – 793893
Dimethyl glutarate	9.2 – 26.6 – 66.6 – 103.2	0.9993	Y= 33068X + 64768
DPGME- Isomer 1	101.7 – 203.4 – 418.8 – 524.8 – 839.6 – 1049.5	0.9984	$Y= 256321X – 2.10^7$
DPGME- Isomer 2	101.7 – 203.4 – 418.8 – 524.8 – 839.6 – 1049.5	0.9992	$Y= 193423X – 1.10^7$

decreases, the relative effect of the amine group increases, which results in stronger sorption to polar stationary phases. In addition, amines tend to decompose in the GC column, and to sorb to exposed parts of the equipment and instrumentation. In general, chromatographic separation of aliphatic amines is much more difficult than separation of aromatic amines.[21]

The quantification of VOC and SCOV was carried out using an external standard method. Different concentrations of the standards were analysed applying the optimized test conditions. Table VIII specifies the linear regression resulting from each standard and its concentrations. The quantification values of the target compounds are indicated in Table IX.

LQ corresponds to the Limit of Quantitation according to the calibration standards curve of the target compounds.

LD corresponds to the detection limit, as no response had been detected from the target compounds.

Table IX

Concentration of the target compounds in the resin samples by HS-SPME/GC-MS.

Resin samples	g/l DPGME (Isomer 1)	RSD (%)	g/l DPGME (Isomer 2)	RSD (%)	g/l Dimethyl adipate	RSD (%)	g/l Dimethyl glutarate	RSD (%)
NV002	15.7	9.8	15.0	9.2	LD < 0.02	-	LD < 0.01	-
NV003	LQ = 10	-	LQ = 10	-	35.7	9.1	1.0	8.9
NV004	LQ = 10	-	LQ = 10	-	68.2	8.6	4.3	7.2
NV005	LD < 0.1	-	LD < 0.1	-	86.2	8.8	6.9	7.9
NV006	LD < 0.1	-	LD < 0.1	-	LD < 0.02	-	LD < 0.01	-
NV007	LQ = 10	-	LQ = 10	--	LD < 0.02	-	LD < 0.01	-
NV008	LD < 0.1	-	LD < 0.1	-	LQ = 3	-	LD < 0.01	-
NV009	LD < 0.1	-	LD < 0.1	-	0.1	9.0	LD < 0.01	-
NV010	44.1	9.7	42.2	8.4	ND	-	LD < 0.01	-
NV011	45.2	9.3	44.7	8.1	ND	-	LD < 0.01	-

Conclusions

The method for the extraction of VOC and SCOV prior to detection by GC-MS in new polyurethane water-based resins for leather finishing using the HS-SPME methodology has been optimized and validated for the determination of the target compounds: Dipropylenglycol monomethyl eter (DPGME) and DBE-3 in the basis of Dimethyl glutarate and Dimethyl adipate. The test method is not viable for TEA, since the peak resolution is poor and with low sensitivity. Next research tasks are focused to determine TEA by TD-GC-MSD.

Acknowledgements

This study has been carried out thanks to the Ministry of Economy and Competitiveness - Collaboration Challenges (MINECO) (Spain) through the NoVocs project "Innovative sustainable leather article free of Volatile Organic Compounds (VOC) and crosslinking agents" RTC-2016-4575-5 and the research entity A3 Leather Innovation Center (University of Lleida) (Catalonia).

References

1. MITECO; Ministerio para la transición ecológica., De compuestos orgánicos volátiles, 2019. [Online]. Available: https://www.miteco.gob.es/es/calidad-y-evaluacion-ambiental/temas/atmosfera-y-calidad-del-aire/emisiones/act-emis/compuestos_organicos_volatiles.aspx#. [Accessed: 18-Mar-2019].
2. RISTOX, "ISTAS: Compuestos orgánicos volátiles (COV)," 2010. [Online]. Available: http://risctox.istas.net/index.asp?idpagina=621. [Accessed: 18-Mar-2019].
3. E. Chorier, N. Blanc, J. C. Cannot, and A. Berthod, Headspace GC-MS for the determination of halogenated hydrocarbons, ethers and aromatic volatiles in fabric and leather, *JALCA* vol. **109**(10), pp. 322–329, 2014.
4. R. M. Cuadros Domènech, Contribució a la caracterització i disminució de l'ús de compostos orgànics volàtils en el sector adober, Universitat Politècnica de Catalunya, 2013.
5. J. W. Allwood and R. Goodacre, An introduction to liquid chromatography-mass spectrometry instrumentation applied in plant metabolomic analyses, *Phytochem. Anal.*, **21**(1), pp. 33–47, Jan. 2010.
6. M. C. Gutiérrez and M. Droguet, La Cromatografía de Gases y la Espectrometría de Masas: Identificación de compuestos causantes del mal olor, *Univ. Politécnica Catalunya*, vol. 122, pp. 35–41, 2002.
7. R. Cuadros, M. Alves, L. Olle, A. Bacardit, and J. Font, Characterization of the volatile organic compounds by HS-SPME-CG-MS in the leather sector., *JALCA* **108**(11), pp. 420–427, 2013.
8. H. Piri-Moghadam, F. Ahmadi, and J. Pawliszyn, A critical review of solid phase microextraction for analysis of water samples, *TrAC - Trends Anal. Chem.*, **85**, pp. 133–143, 2016.
9. G. Ouyang and J. Pawliszyn, SPME in environmental analysis, *Anal. Bioanal. Chem.*, **386**(4), pp. 1059–1073, Oct. 2006.
10. M. H. Tunick, S. K. Iandola, and D. L. Van Hekken, Comparison of SPME Methods for Determining Volatile Compounds in Milk, Cheese, and Whey Powder., *Foods (Basel, Switzerland)*, **2**(4), pp. 534–543, Nov. 2013.
11. H. Lan *et al.*, Modified zeolitic imidazolate framework-8 as solid-phase microextraction Arrow coating for sampling of amines in wastewater and food samples followed by gas chromatography-mass spectrometry, *J. Chromatogr. A*, **1486,** pp. 76–85, Feb. 2017.
12. A. Marsol-Vall, J. Eras, M. Balcells, B. Sgorbini, C. Cagliero, and C. Bicchi, Volatile composition and enantioselective analysis of chiral terpenoids of nine fruit and vegetable fibres resulting from juice industry by-products, *Hindawi J. Chem.*, **2017**, pp. 1–11, 2017.
13. MERCK, SPME for GC analysis, *Supelco*. pp. 1–28, 2018.
14. M. R. Reyes Ferrera, Determinació de fungicides en pells i en banys de procés del sector adober, Universitat Politècnica de Catalunya, 2015.
15. V. López-Grimau and M. C. Gutiérrez, Detección por GC-MS de Trimetilamina como causa del mal olor, *Univ. Politécnica Catalunya*, **128**, pp. 39–44, 2005.
16. OECD, Introduction Dipropylene Glycol Methyl Ether CAS N ° : 34590-94-8 (Isomers : 13429-07-7 , 20324-32-7 ; 13588-28-8 and 55956-21-3). UNEP PUBLICAIONS, pp. 1–99, 2001.
17. Kumbra Trading CO. LTD, What is Kumra making with it?, 2004. [Online]. Available: http://kumra.co.kr/3_produ02_4.html. [Accessed: 17-Feb-2020].
18. The Dow Chemical Company, Product Safety Assessment: ESTASOL™ Oxygenated Solvent Manufacture of Product, 2009. [Online]. Available: http://www.multisolgroup.com/Estasol-. [Accessed: 17-Feb-2020].
19. J. Torrens, M. Riu-Aumatell, E. López-Tamames, and S. Buxaderas, Volatile compounds of red and white wines by headspace-solid-phase microextraction using different fibers., *J. Chromatogr. Sci.*, **42**(6), pp. 310–6, Jul. 2004.
20. V. Gyorgy, Vas; Karoly, Solid-phase microextraction: a powerful sample preparation tool prior to mass spectrometric analysis, *J. MASS Spectrom. J. Mass Spectrom*, **39**, pp. 233–254, 2004.
21. J. Namieśnik, A. Jastrzębska, and B. Zygmunt, Determination of volatile aliphatic amines in air by solid-phase microextraction coupled with gas chromatography with flame ionization detection, *J. Chromatogr. A*, **1016**(1), pp. 1–9, Oct. 2003.
22. E. Lemazurier, A. Lecomte, F. Robidel, F. Bois, Propylene glycol monomethyl ether. A three-generation study of isomer B effects on reproductive and developmental parameters in rats. Toxicology and industrial health. **21**, 33-40. 10.1191/0748233705th213oa. 2005

COLD
Milling

Smooth Leather Milling

Erretre
Tannery Innovations

Erretre s.p.a. | Via Ferraretta,1 | Arzignano (VI) 36071 | tel. +39 0444 478312 | info@erretre.com

Lifelines

Hu Lianhua, associate professor of Shaanxi University of Science and Technology, Doctor of Engineering, mainly engaged in the research work of measurement and control algorithm, modeling and simulation, DCS & QCS system design for pulping and papermaking process.

Xiang Chengyi, Master candidate at the School of Mechanical and Electrical Engineering, Shaanxi University of Science and Technology, mainly interested in digital image processing, computer vision, machine learning and data fusion.

Zhang Feng, associate professor in Shaanxi University of Science and Technology. His research interests include application research of new technology and new equipment in pulping and papermaking process, design theory and application research of power machinery. Fluid machinery and numerical simulation technology; energy saving technology of thermal power system.

Zhen Wang received his B.S. degree in Light Chemical Engineering at Sichuan University in 2019. Now he is pursuing his master's degree in Biomass Chemistry and Engineering at Sichuan University. His research focuses on chrome-free tanning technology.

Ya-nan Wang received his Ph.D. degree in Leather Chemistry and Engineering at Sichuan University in 2013. After graduating, he joined Sichuan University as a lecturer. Now he is a professor in National Engineering Research Center of Clean Technology in Leather Industry, Sichuan University. His research focuses on chrome-free tanning chemistry and technology.

Yue Yu, see *JALCA* **115**, 190, 2020.

Bi Shi, see *JALCA* **99**, 220, 2004.

Nan Chen, is a master student in School of Light Industry and Engineering in Qilu University of Technology (Shandong Academy of Sciences), her research focuses on the application of electrospinning technology in leather field.

Yanchun Li, professor of School of Light Industry and Engineering in Qilu University of Technology (Shandong Academy of Sciences), who is expert of research on cleaner production technology and theory for tannery.

Jianbo Qu, professor of School of Light Industry and Engineering in Qilu University of Technology (Shandong Academy of Sciences), his research focuses on the Functional polymer materials.

Jian-Yong Wang, professor of School of Light Industry and Engineering in Qilu University of Technology (Shandong Academy of Sciences), his research interests cover the interdisciplinary areas of functional organic molecules and polymers construction, molecular recognition and chemical biology.

Antonia Flores Reyes, Industrial Technical Engineer, specialty in Industrial Chemistry, in 2010 from the UPC. In 2016 she completed the Master's Degree in Leather Engineering also at the UPC. She is currently doing a doctorate in the Engineering and Information Technology program at the UdL. She at a professional level from 2012 to 2015 she worked in the quality department of Simar, S.A. and from 2016 to 2018 she worked in research at A3 Leather Innovation Center, participating in the GrapeTan and NoVOCs projects.

Sílvia Sorolla, Technical engineering in Chemical Industry UPC (1997). Master in Leather engineering UPC (2010). Ph.D. in Chemical Engineering by UPC (2011). Her scientific and technical professional background has been developed in different fields, starting as researcher in AIICA Technological Center, from 1997 to 2012. In 2004, she started working as the coordinator of the technical activities within the research projects (DERMAGENESIS, 6th FP). She collaborated as researcher in other R&D projects (5,6th FP, LIFE, Eurostars). She also worked in the development of research proposals, Consortium Agreements and Collaboration Agreements with companies. She developed the task of Project Manager from 2009 to 2012. Since 2012 to September of 2018, she developed her professional activity in the A3 Chair in Leather Innovation (UPC), being her activities focused on the field of the development of R&D projects at National and EU level, developing both technical managing and experimental work.

C. Casas graduated in Industrial Engineering Chemical at the Universitat Politècnica de Catalunya (Spain) in 1986. She received the Master in Tanning Technical Management from the Universitat Politècnica de Catalunya (Spain) in 2012. From 1986 to 1988 she worked in the Engineering Department at Majosa in Prat de Llobregat (Spain). From 1988 to 2008 she worked as Quality manager at Hisitex in Igualada (Spain). Since 2009 she has been working as a Researcher and Project manager first at AIICA and currently at A3 Chair in Leather Innovation from the Igualada Engineering School (Universitat Politècnica de Catalunya). She is mainly involved in the development of R&D projects at National and European level.

Rosa Cuadros, graduated in Technical Industrial Chemistry Engineering at the Technical University of Catalonia (Spain) in 1993. From 1993 to 1996 she has been working in a laboratory for analysis and research, AIICA (Spain). Since 1996 she has being working as a lecturer at the Igualada Industrial Engineering Technical School – Igualada Tanning School at the Technical University of Catalonia. Since 2006 has a degree in technical research and marketing by the Open University of Catalonia. She is mainly involved in environment, safety, quality and communication research projects.

A. Bacardit graduated in Industrial Engineering Organization at the Universitat Politècnica de Catalunya (Spain) in 2003. She got the Ph. D. degree in Chemistry at the University of Barcelona in 2005. She received the Master in Tanning Technical Management from the Universitat Politècnica de Catalunya (Spain) in 2001. From 1995 to 1999 she worked in the Technical Laboratory at BASF-Curtex in L'Hospitalet (Spain). Since 1999 she has been working as a lecturer at the Universitat Politècnica de Catalunya. Since September 2018 is professor at the Universitat de Lleida. She is mainly involved in the development of cleaner and innovative leather processing methods.

INDEX TO ADVERTISERS

116th ALCA ANNUAL CONVENTION
Change of Date:
June 21–24, 2022
Eaglewood Resort & Spa
Itasca, IL

Featuring the 61st John Arthur Wilson Memorial Lecture
By Randy Johnson, President and CEO
of GST AutoLeather
Title: Road Ahead

Tentative Schedule

Tuesday, June 21
Golf Tournament, Opening Reception and Dinner

Wednesday, June 22
John Arthur Wilson Memorial Lecture
All Day Technical Sessions, Fun Run
Reception and Dinner, Activities - Bowling, Pool,
Darts and an Open Bar

Thursday, June 23
All Day Technical Sessions, Annual Business Meeting
Activities Awards Luncheon
Social Hour, ALCA Awards Banquet

Visit us at www.leatherchemists.org for full details
under Annual Convention as they become available

CHEMTAN

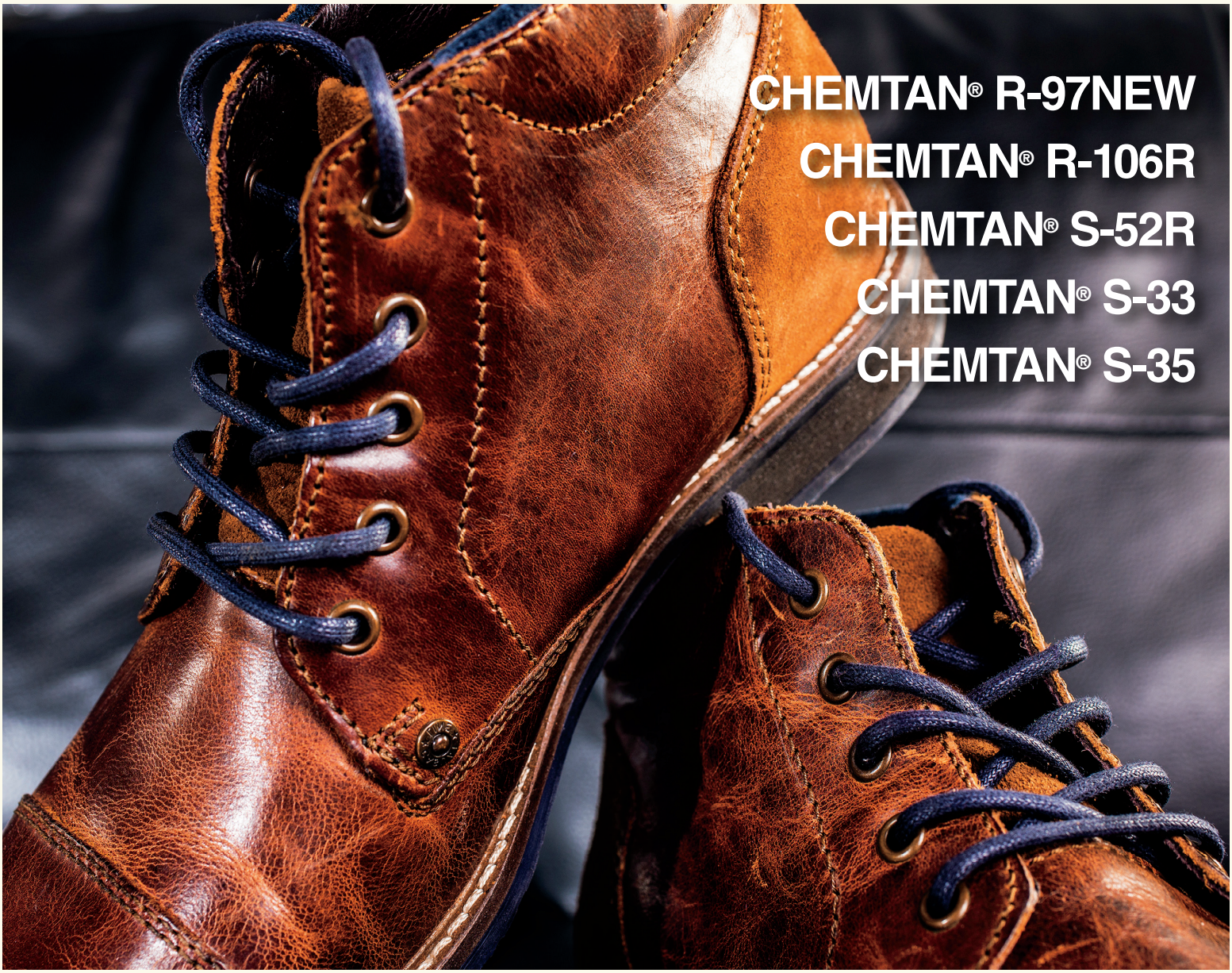

Weatherproof. Built to Last.

Tel: (603) 772-3741 • www.CHEMTAN.com